Electrochemical Biosensor: Multistep functionalization of thiolated ssDNA on gold-coated microcantilever

Jorge Dulanto Carbajal

Department of Phisics

McGill University

Montréal, Québec

September, 2011

A Thesis submitted to

McGill University

In partial fulfillment of the requirements for the degree of

Master in Science

Acknowledgements

This thesis is dedicated to my mother Ana, my father Jorge, my brother Renzo and his family who always supported me during this challenge.

I would like to thank my supervisor Peter Grütter who gave me this amazing opportunity to learn and to live Physics. Thanks also goes to Yoshihiko Nagai 'Tigre' who taught me almost everything I know about this project. I would also like to thank James Hedberg for his help in the proof-reading of this thesis.

Thanks to all my friends in the Physics department who always gave me energy to complete this wonderful period of my life.

Table of Contents

Abstract:

Bio-chemical sensors are an emerging and vibrant area of research. The use of micromechanical cantilevers is relatively new as biomechanical recognition detectors. Reactions on a gold coated and chemically functionalized surface produce a mechanical deflection of the cantilever which is used as the input signal of the detector. Within the area of biosensors, DNA-sensors have a wide range of applications such as DNA hybridization detectors, DNA mismatch sequence detectors and protein detectors.

We designed and built a microcantilever sensor system which allows for control and characterization of surface conditions. This includes controlled functionalization which can be a dominant factor in signal generation and reproducibility in these systems. Additionally, we developed a multistep functionalization protocol which consists of a sequence of short incubations and characterizations of thiolated ssDNA on a gold-coated cantilever.

Multistep functionalization is a new protocol that is used to control the ssDNA surface density on a gold-coated cantilever. Repeatable responses and feasible biosensors are obtained using this protocol.

Résumé:

Les capteurs biochimiques sont un domaine émergent et dynamique de la recherche. L'utilisation de cantilevers micromécaniques est relativement récente en tant que détecteur par reconnaissance biomécanique. Des réactions sur la surface recouverte d'or et fonctionnalisée chimiquement produisent une déviation mécanique du cantilever qui constitue la source de mesure du détecteur. Dans le domaine des biocapteurs, les capteurs d'ADN ont un large champ d'application tel que les détecteurs d'hybridation d'ADN, les détecteurs de mésappariement d'ADN et les aptamères (détecteurs de protéines).

Nous avons conçu et construit un système de capteur microcantilever permettant le contrôle et la caractérisation des conditions de surface. Une fonctionnalisation contrôlée est un facteur dominant pour la génération de signal et de la reproductibilité dans ces systèmes. Afin d'atteindre cet objectif, nous avons développé le protocole de fonctionnalisation en plusieurs étapes qui consiste en une séquence d'incubations de courte durée (5min chacune) et de caractérisations d'ADN simple brin thiolé sur le cantilever recouvert d'or.

La fonctionnalisation en plusieurs étapes est un nouveau protocole qui contrôle la densité de surface d'ADN simple brin sur cantilever recouvert d'or. Des réponses reproductibles et des biocapteurs faisables sont obtenus grâce à ce protocole.

1 Introduction

1.1 Motivation

Bio-chemical sensors are an emerging and vibrant area of research. The use of micromechanical cantilevers as detectors, sensitive to biological species has been investigated in the past 10 years. A new subgroup of biosensors is the DNA (deoxyribonucleic acid) sensors which are capable of detecting DNA hybridization [1-2], mismatches in the DNA sequence [3-5], and specific proteins. DNA aptamers are used to detect proteins [1, 6]. In this thesis, we will discuss and analyze the DNA hybridization detector.

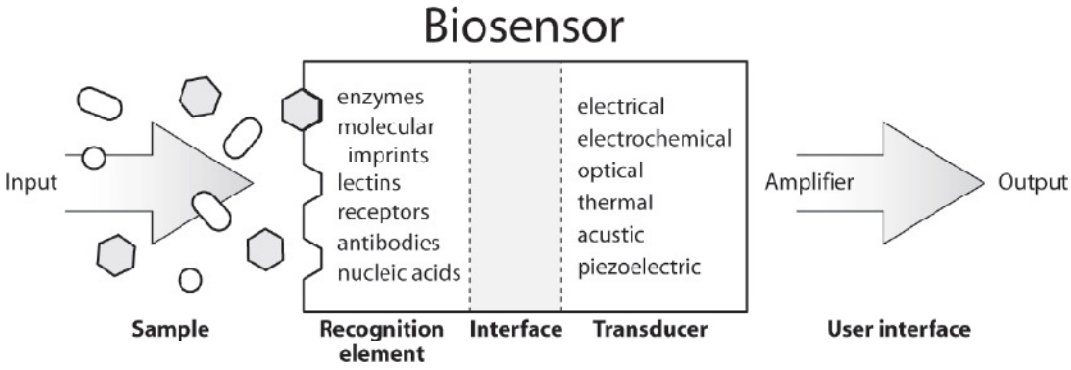

Figure 1.1: Elements and selected components of a typical biosensor [7]

Most generally speaking, a biosensor is composed of the recognition element, the interface, and the transducer as shown in figure 1.1. The sample is recognized by the recognition element, and the transducer converts the chemical stimulus into a measurable output signal. The sample is also known as the analyte, the recognition

element as the chemical layer, and the transducer as the physical transducer. The chemical layer and the transducer limit the performance of biosensors. Previous work has often focused on the limits of the transducer. However, this research seeks to improve the recognition element. In cantilever-based surface stress sensors, we pay special attention to the surface density conditions of the thiolated single-stranded DNA (ssDNA) monolayer [6]. The ssDNA layer on the gold-coated side of the cantilever serves as the recognition element while the cantilever serves as the transductor.

We find that the DNA sensor's response is highly dependent on the thiolated ssDNA surface density. For this reason a new functionalization protocol is developed. The multistep functionalization protocol permits control over the thiolated ssDNA surface density [8]. By studying the evolution of the cantilever's surface stress response after a series of short incubations, we discover the physical origins that change the adsorption and desorption conditions under electrochemical stimulation. This thesis investigates several fundamental issues relevant to micromechanical detection of DNA hybridization: adsorption and desorption processes and the factors that affects on them. This understanding will improve reproducibility and allow for the optimization of the response signal of the biosensor.

1.2 Micromechanical cantilever-based sensor

Microcantilever-based sensors respond to changes on their surface or in their environment with a mechanical bending. This mechanical bending is in the order of nanometers which is easy to detect without amplification. In the other hand, electrochemical DNA sensors take advantage of nanoscale interactions between the

solution, the recognition layer and the solid electrode to develop sensitive, selective and low cost DNA sensors. In our DNA sensor, we combine both types of DNA sensor, maximizing its performance.

In DNA microarray techniques (Gene Chip), a fluorescence readout is used which involves not only highly precise and expensive instrumentation but also sophisticated numerical algorithms to interpret the data. This condition limits their use to research laboratories.

In our DNA sensor, an adsorbate layer on the cantilever produces a reconstruction of the cantilever surface and surface-liquid interface that creates surface stress. This surface stress produces deflection in the cantilever which is our variable to measure.

The mechanical deflection of a gold-coated cantilever due to receptor-ligand interaction was first reported by researchers at IBM Zurich [9]. An adsorbed layer of thiolated ssDNA is formed on the gold-coated surface of the cantilever. A complementary solution-based ssDNA is subsequently added. The resulting DNA hybridization process produces a change in the deflection of the cantilever [10]. The surface stress changes have been attributed to steric hindrance, electrostatic repulsion, Van der Waal's forces, counterions pressure and hydration forces between DNA strands [9, 11-14]. Contradictory results with respect to the direction and the magnitude of the stress appear in further studies [1, 14-15]. These contradictory results show an incomplete understanding of cantilever-based sensors. To understand the deflection in our hybridization detector, we focus on the following:

a) Adsorption and desorption processes.

b) Potential of zero charge: V_{pzc}.

c) Mechanical and electrical properties of thiolated ssDNA and double-stranded DNA (dsDNA).

The potential of zero charge is the potential with respect to the reference electrode that describes the condition when the electrical charge density on the surface of the working electrode (in our case the gold surface) is zero. This concept is associated to the phenomenon of adsorption [16].

These three factors are closely related. The adsorption and desorption rate are different if the potential of zero charge, $V_{pzc,}$ changes. The mechanical and electrical properties of the thiolated ssDNA or dsDNA monolayers vary the electrical conditions of the gold-coated surface, for example, the potential of zero charge V_{pzc} [17-18].

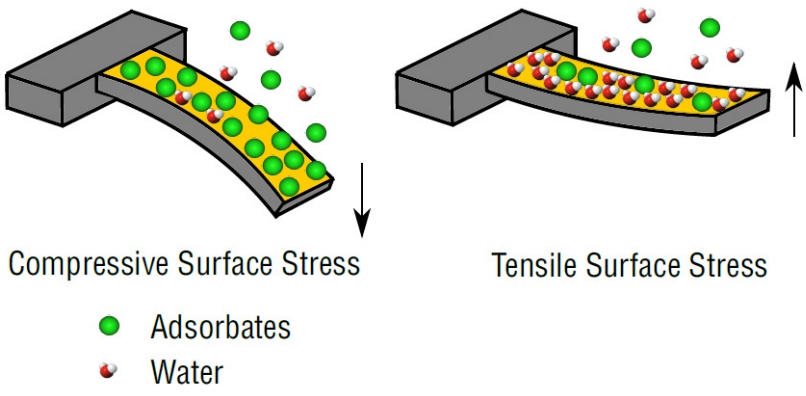

Figure 1.2: Compressive and tensile surface stress on cantilever.

Figure 1.2 shows a representation of the adsorption and desorption of the adsorbate ions (Chloride ions in our buffer). Compressive and tensile surface stress can both be present. Another process that requires analysis is the double layer formation which is an arrangement of the cations and anions on the electrodes. The double layer can be modeled as an electric capacitor [19-20].

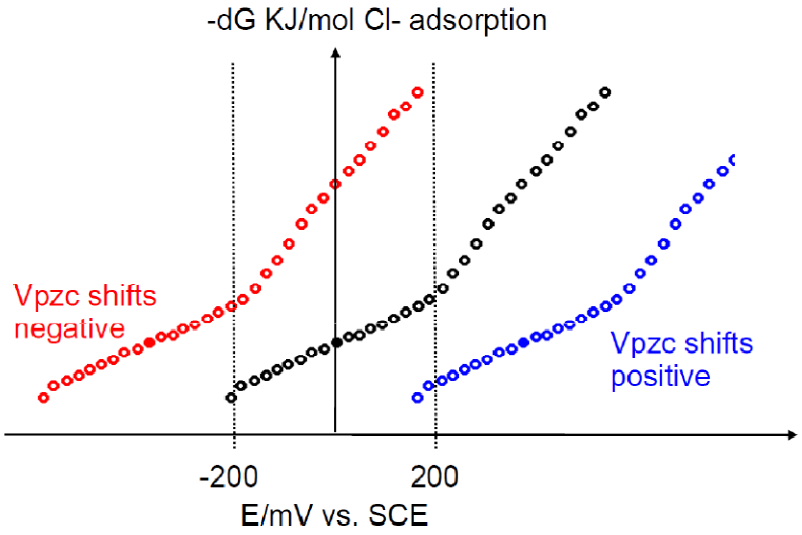

Fig. 1.3: Energy of adsorption vs. potential (mV vs. SCE). Adapted from [21]

Figure 1.3 shows in black the curve of adsorption energy of chloride (Cl^-) vs. potential with respect to saturated calomel electrode (SCE) based on data from J. Lipkowski et al [21]. The red and blue curves represent the new conditions of the adsorption energy under a positive or a negative shift of the V_{pzc} on the gold surface. Both, positive and negative shift on the potential of zero charge (V_{pzc}) are presented in our detector due to new surface conditions (charge distribution, dipole moments on thiolated DNA). These adsorption and desorption are different between ssDNA and dsDNA monolayers due to differences in electrical and mechanical properties. Different conditions for the adsorption and desorption between a ssDNA monolayer and a dsDNA monolayer, result in different surface stress responses. This is the goal of our hybridization detector.

This thesis is developed as follows: Chapter 2 focuses on the instrumentation and the electrochemical methods that we used in our experiments. Chapter 3 gives an introduction about organothiol monolayers and surface stress on gold surfaces. In

chapter 4, we explain the experiments used to develop the multistep functionalization protocol. We analyze the phenomena over the gold surface with thiolated DNA and how we used it to develop our hybridization detector. Chapter 5 contains the conclusions and outlook. Appendix A presents a useful procedure to prepare thiolated ssDNA sample, appendix B shows the design and evaluation of a new electrochemical cell and appendix C gives an introduction about dipole moments on DNA nucleotides.

2: Instrumentation and methods

Chapter 2 describes the apparatus and the electrochemical methods used to perform electrochemical biosensiong experiments. The electrochemical apparatus is based on a three-electrode potentiostat. The two electrochemical techniques used in our experiments are cyclic voltammogram and square wave potential (adapted from chronoamperometry). The cantilever deflection is measured by the laser deflection method.

2.1 Electrochemical setup

The electrochemical setup is based on a three-electrode potentiostat. Figure 2.1 shows the schematic of the three-electrode system.

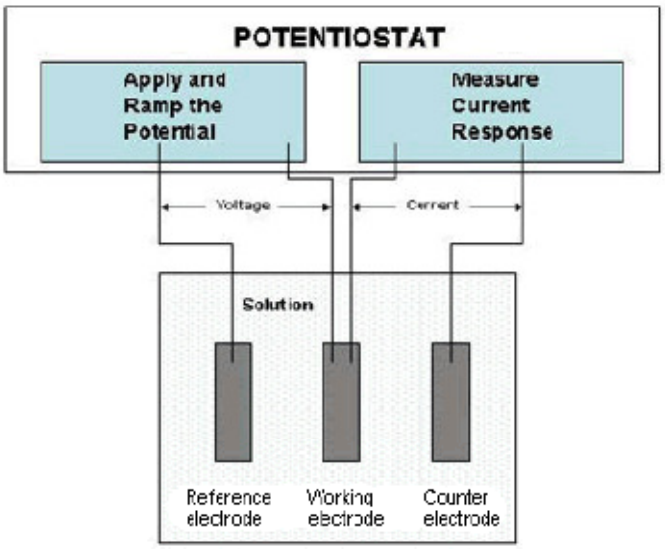

Figure 2.1: Potentiostat with the three electrode configuration for performing electrochemical measurements [22].

2.1.1 Electrodes

2.1.1.1 Reference electrode (RE)

The reference electrode is an electrode with a stable and well-known electrode potential. A standard calomel Ag/AgCl is used as reference electrode. The properties of this reference electrode are: Stable potential of 0.242 V vs. normal hydrogen electrode (NHE) [23]. The reference electrode has a negligible current to avoid a drop in the potential. This minute current is due to the high impedance between the working electrode and the reference electrode. For that reason the reference electrode is built in a way that its environment doesn't change (inert condition). In the three electrode system, the use of a counter or auxiliary electrode is used to protect the reference electrode.

An alternative electrode is the pseudo reference electrode which consists of a silver (Ag) wire coated with silver chloride (AgCl). This electrode is appropriate for miniaturization of the electrochemical cell [24]. The pseudo reference electrode shifts the reduction peak potential to more negative potential until it reaches a fixed value.

2.1.1.2 Counter electrode (CE)

We use a platinum wire as a counter (or auxiliary) electrode. The current passes across the working electrode and the counter electrode, permitting the reference electrode to keep its high impedance condition. The electrochemical properties of the platinum wire do not affect the behaviour of the electrode of interest (working electrode) because platinum is an inert material. Usually the counter electrode is much

larger than the working electrode. The potential is smaller between the working electrode and the reference electrode than between the working electrode and the counter electrode. The three-electrode system works as a potential divider in a potentiometer [25].

2.1.1.3 Working electrode (WE)

All the processes of interest occur on the working electrode. We use a gold-coated Mikromash (CSC12 tipless / without Al) [26] microcantilever as a working electrode. This microcantilever allows us to measure optically its deflection in parallel with the electrochemical measurements. Thiolated DNA self assembly monolayer (SAMs) on gold are well-known due to the stable chemisorbed link between the gold and the sulphur end of the thiol group [27].

It is difficult to isolate the gold-coated microcantilever from its electric connector. The epoxy glue (figure 2.2) improves significantly this isolation in our experiments. The meniscus setup and the delicate manipulation of the microcantilever are eliminated, optimizing the time in our experiments and the lifetime of the microcantilevers.

Some of the properties of the epoxy glue (Eccobond 286 [28]) are: 1.0 W/m.K of thermal conductivity, a minimum of 10^{14} Ohm.cm of volume resistivity and, an excellent chemical and solvent resistance [28].

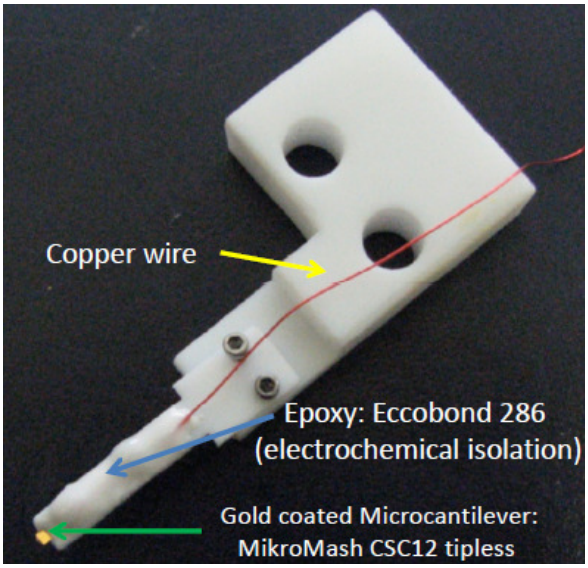

Figure 2.2: Microcantilever setup.

2.1.2 Electrochemical cell

The material for the construction of the electrochemical cell is polytetrafluoroethylene (PTFE), also well-known as Teflon. This material is an excellent electrochemical inert material that also poses a high thermal resistivity. These conditions avoid any unwanted reactions on the cell. Figure 2.3 shows the entire electrochemical setup, which was designed and built as part of this thesis. The (electrochemical) cell has two glass windows that permit the travel of a laser beam (in an out) for the optically measurement of the cantilever's deflection. This electrochemical cell has a large enough volume (~3ml) that eliminated thermal drift phenomena [29].

Figure 2.3 shows our one-cantilever electrochemical setup. This configuration can be upgraded to a two-cantilever configuration to perform more sensitive experiments where larger fluctuations in temperatures and nonspecific reactions are non-negligible [29-30]. Due to epoxy coverage (Eccobond 286) the cantilever can be submerged completely, and the pressure of argon gas introduced during the gold surface cleaning process can be higher. As a result, unwanted oxidation is minimized and better defined, clean gold surfaces are obtained.

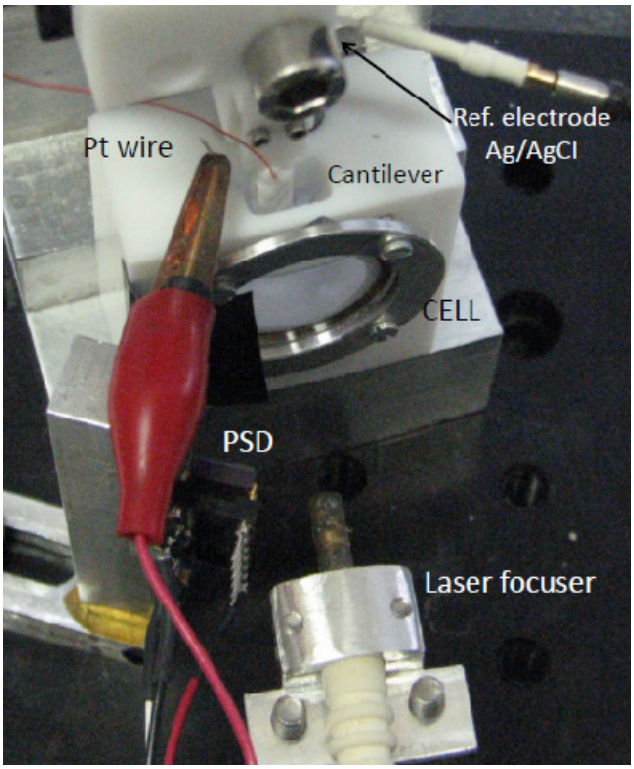

Figure 2.3: one-cantilever mode: electrochemical setup.

The microcantilever is clamped with a beryllium-copper clip which serves to hold it in the groove of the Teflon rod, and to make electrical contact with the gold-coated side of the cantilever. This beryllium copper clip is covered with epoxy glue. In order to ensure that the laser beam deflects onto the PSD, the groove of the Teflon rod is positioned at 15° with respect to the glass slides as figure 2.4 shows.

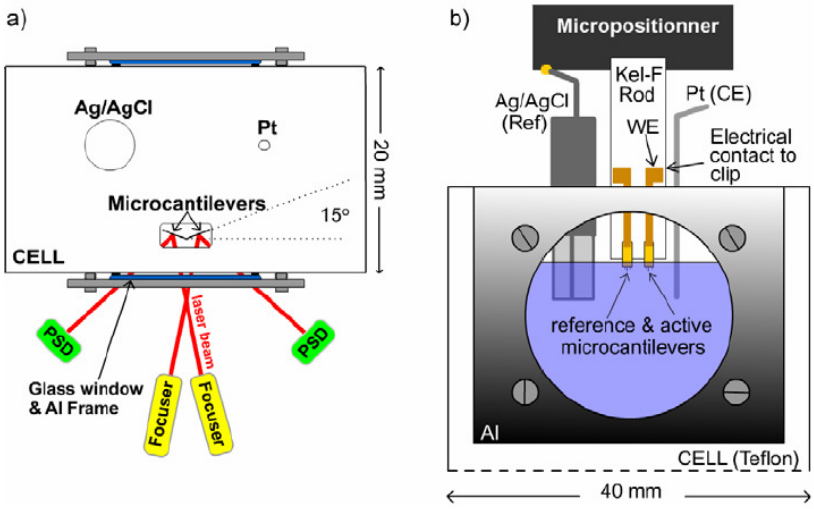

Figure 2.4: Schematic of electrochemical cell for two cantilever setup [30].

2.1.3 Apparatus specifications:

Reference electrode:	3M Ag/AgCl, MF-2078 from BASi
Counter electrode:	Platinum wire, MW-4130 from BASi
Electrochemical cell:	Teflon, 40mm x 45mm x 20mm, inner diameter = 20 mm, V= 6mm^3
Working electrode: model	Gold coated cantilever, 350µm x 35µm x ~1µm, MikroMash CSC12/tipless/without Al, k=0.03N/m
Clamp for WE:	Teflon, Beryllium-Copper clips
WE isolation:	Epoxy glue: Eccobond 286 (part A and part B)
Laser diode:	635nm, constant current source or constant power source, FMXL112 from FiberMax

2.2 Electrochemical techniques

Prior to performing electrochemical experiments the platinum CE was flame annealed and quenched with Milli-Q water (18.2 MΩ, Millipore Co.). This was performed once per day during experiments. Anytime the electrolyte in the cell was changed the RE was rinsed thoroughly in Milli-Q prior to insertion to prevent any extra chloride ions from being introduced into the cell. The cell was rinsed 3 times with Milli-Q water and 3 times with the electrolyte required for the experiment.

2.2.1 Cyclic Voltammetry

A cyclic voltammogram (CV) is recorded by a three-electrode system which consists of a working electrode (WE), reference electrode (RE) and a counter electrode (CE). These electrodes are inside the analyte and connected to a potentiostat [31].

In cyclic voltammetry, the potential of the working electrode is ramped linearly versus time. The potential ramp is inverted when the working electrode's potential reaches the maximum potential programmed, forming a triangular function (figure 2.5a). The current between the working and the counter electrodes is measured and plotted vs. the applied potential between the working and reference electrodes. The forward scan results in a current peak for analytes in solution that can be reduced.

Cyclic voltammetry measurements look at redox (reduction-oxidation) processes of an analyte in solution. Additionally, these measurements give the information if it is a reversible, quasi-reversible or irreversible process.

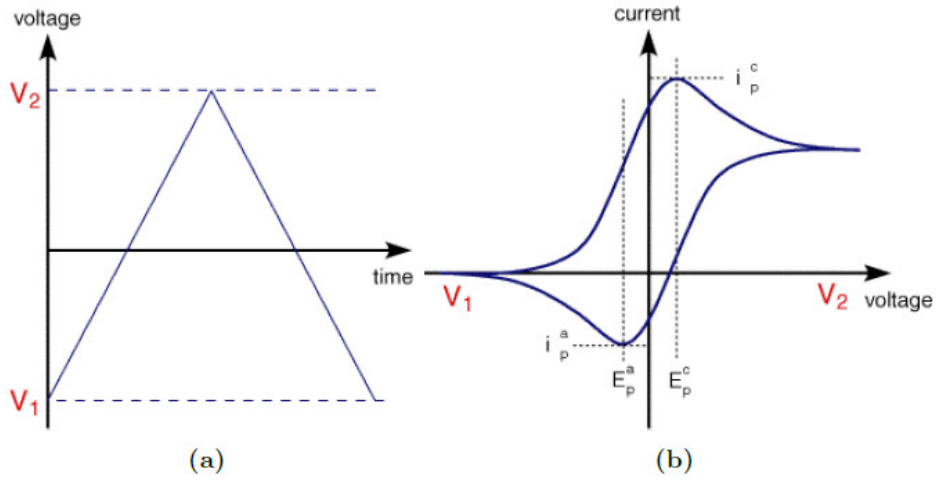

Figure 2.5: (a) Voltages vs. time graph of one cycle. The voltage is ramped linearly versus time until V2 and is then inverted. In (b) the corresponding one cycle CV is shown with the anodic and cathodic peaks [32].

Figura 2.5(b) shows a typical CV. As an example, the redox process for Fe^{3+} / Fe^{2+} described as:

$$Fe^{3+} + e^{-} \leftrightarrow Fe^{2+} \qquad 2.1$$

In figure 2.5a, the voltage is ramped versus time from V_1 to V_2, resulting in a current peak I^{e}_{p} in the CV (figure 2.5). In the negative to positive potential ramping, the current peak corresponds to the oxidation reaction of Fe^{2+} to Fe^{3+}. When the potential is shifted further to more oxidative values, the electrons begin to move a more Fe^{2+} is converted into Fe^{3+}. In the case of inverted potential ramping (from V_2 to V_1), the CV shows a second current peak i^{o}_{p} from the reduction process. In the case that the peaks are symmetric the reaction is reversible. If the current peak is slightly drifted apart, the reaction is quasi-reversible, and, if the current peaks are totally drifted apart or just with one peak visible, the reaction is irreversible [33].

Additionally information can be obtained changing the voltage scan rate. An increase of the voltage scan rate produces an increase in the current peaks. By analysing the variation of the peak positions as a function of the scan rate, it is possible to gain an estimation of the electron transfer rate constant [34].

For our purpose, electrochemistry is used to gain higher reproducibility and control by using well-defined electrochemical cleaning procedures, electrochemical characterization and well-defined measurement cycles. The initial state can be characterized with electrochemistry leading to the same initial conditions for each experiment. We clean the Au surface of the coated cantilever by a CV in 50 mM KClO4 from -800 to +1300 mV.

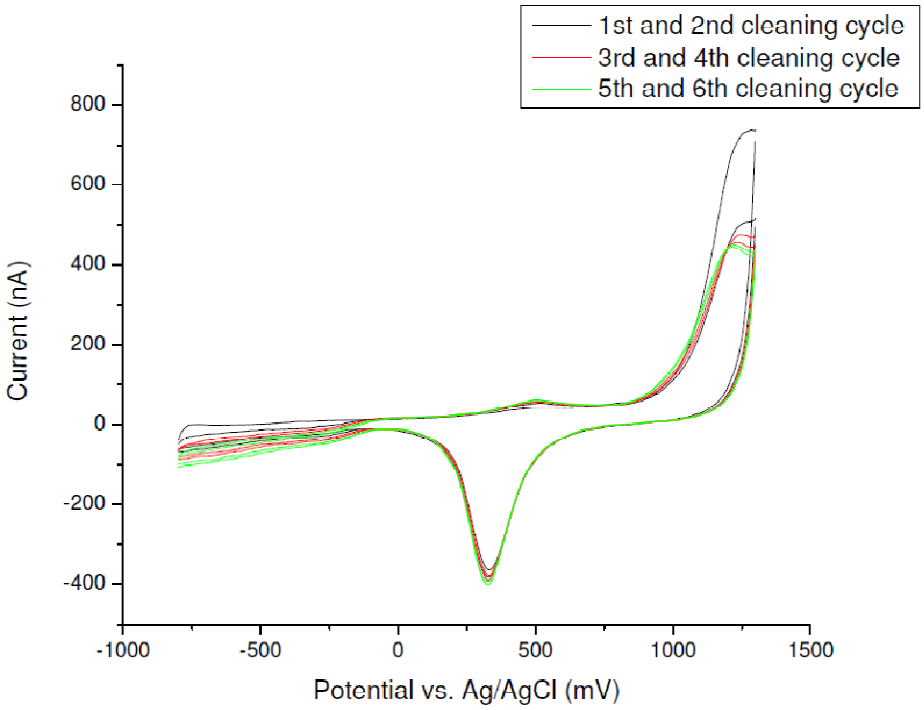

Figure 2.6: Cleaning steps of gold surface (microcantilever) by cyclic voltammetry (CV)

Figure 2.6 shows the evolution of the cyclic voltammogram when the cantilever's gold surface is cleaning. Black, red and green trace are consecutive cleaning

(four complete sweeps or 2 cycles of the potential range by each figure) using cyclic voltammetry applied to the same gold-coated microcantilever. The surface is considered clean when a smooth and reproducible cyclic voltammogram is obtained, indicating a homogeneous, stable, and equilibrated surface [35]. For all cases, a sweep rate of 20mV/sec is applied.

After cleaning, a subsequent evaluation of an additional use of the cyclic voltammetry method is to evaluate the surface stress change vs. potential (vs. Ag/AgCl) is performed to establish that the initial starting clean Au surfaces show quantitative reproducibility. If the measured stress is not within +/- 10% of our average values (~165 mN/m) using a TN buffer (Tris-HCl 10mM NaCl 50 mM) we repeat the cleaning or discard the cantilever.

2.2.2 Square wave potential (Chronoamperometry)

In order to observe some interesting time dependant phenomena caused by our DNA thiolated monolayer we perform a square wave potential protocol. This protocol is an adaptation of the electrochemical protocol chronoamperometry. Square wave potential allows us to observe the time constants of change in the adsorption and desorption processes (specifically of DNA dynamics and chloride ions) when some potential transitions is applied onto the cantilever's gold surface.

The chronoamperometry is an electrochemical technique where the potential applied to the working electrode is stepped. These potential steps generate a transient of high current that decays, similarly to the behaviour of a RC circuit [36-37].

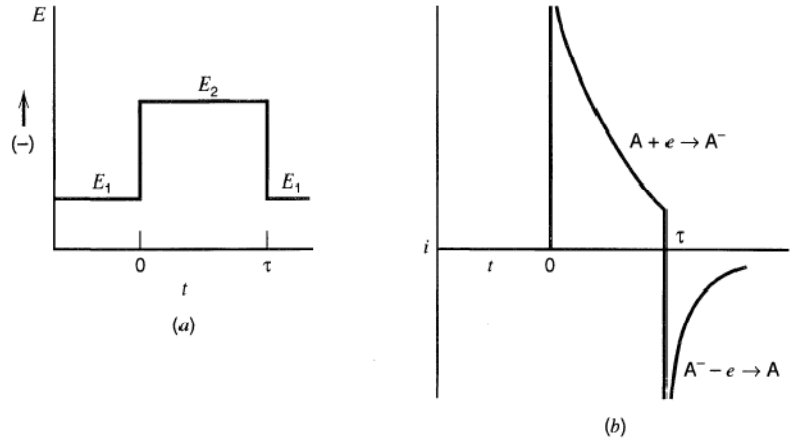

Figure 2.7: Double potential step chronoamperometry: (a) Typical waveform (b) Current response [36].

The experiment shows in figure 2.7 is called double potential step chronoamperometry and it is an example of a reversal technique. Reversal methods are a powerful arsenal for studies of complex electrode reactions [38].

We adapt the double potential step chroamperometry using a 10 min period square wave that goes from -200 mV vs. Ag/AgCl to +200 mV vs. Ag/AgCl. These conditions reduce the transient current peaks due to Faradaic currents that are disadvantageous for our experiment. The square wave potential protocol and cyclic voltammetry are the two fundamental electrochemical tools to perform and analyze our biosensor experiment.

2.2.3 Double layer structure

The interactions between the electrolyte and the solid electrode are different to those in the solution. Electrodes that are under potentiostat control have an additional effect due to charge at the electrode. These factors produce strong interactions between

ions or molecules (solution) and the electrode surface. As a result, a region called "electrical double layer" appears between the electrode and the solution [39]. Helmholtz was the first to introduce the term 'electrical double layer'. His model assumes that the solution is composed only of electrolyte and no electron transfer reactions occur at the electrode. Interactions between the electrode and the ions in the solution are exclusively electrostatic in nature. The electrode carries either an excess or deficiency of electrons on the electrode surface. To remain neutral, a redistribution of ions in solution close to the electrode balances the electrode charge.

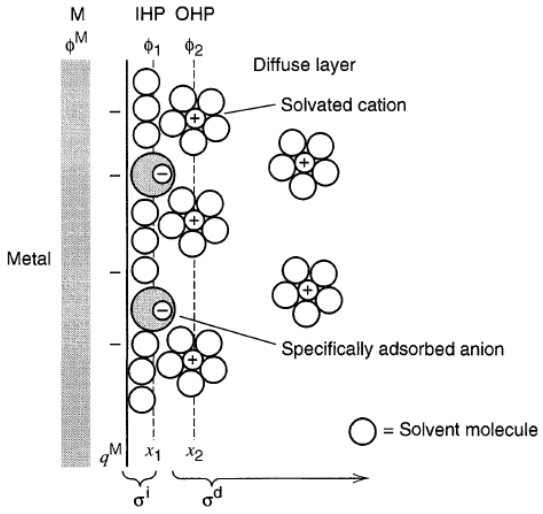

Figure 2.8 Double-layer region when anions are adsorbed [40]

The distance between this ions layer and the electrode surface is limited to the radius of ions and its solvation sphere. As a final result, we obtain two layers of charge (the double layer) and an associated potential drop confined to this region, which is called inner 'the outer Helmholtz plane' (OHP). The Helmholtz model or electrical double layer is analogous to a capacitor with two plates of charge separated by a certain distance. The potential drop behaves linearly between the two plates. In electrochemical

systems, the impedance analysis due to the response of the electrolyte redistribution is thus modelled in terms of capacitance elements.

The model of Helmholtz does not consider some factors such as the possibility of adsorption of ions onto the surface, the diffusion and mixing in the solution, and the interaction between the solvent dipole moments and the electrode. Stern provided a new model that begins to take in account some of these limitations [41].

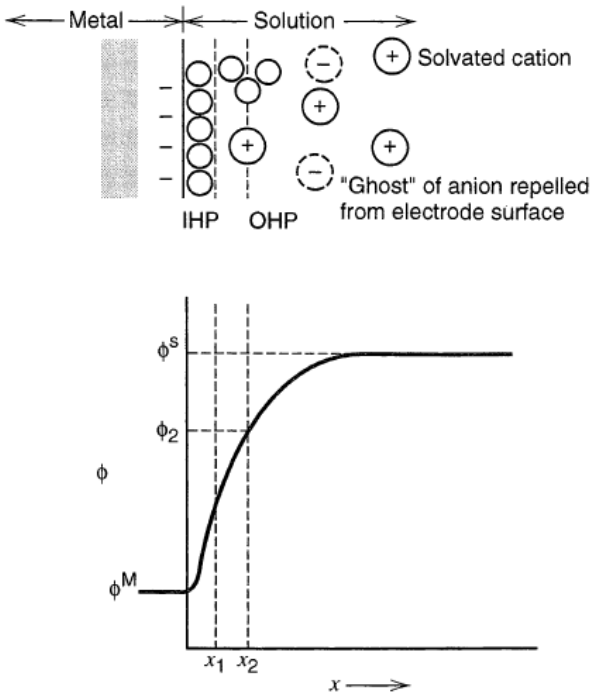

Figure 2.9: Potential profile across the double-layer without adsorption. [40]

The Stern's model assumes that the ions are able to move in solution and the electrostatic interactions are in competition with the Brownian motion. Under these assumptions, there is a region close to the electrode surface ($100x10^{-10}$m) containing an excess of one type of ions and a second region that also has a potential drop called the

diffuse layer (figure 2.8). A detailed description of the double layer structure is found in [41].

2.2.4 Potential of zero charge: V_{pzc}

The potential of zero charge is a characteristic value of the electrode potential where the metallic surface of the electrode will not acquire an electrical charge when it is in contact with an electrolyte [42].

In an electrochemical system, if the applied potential is positive with respect to the potential of zero charge (V_{pzc}), then negative ions are attacted to the electrode from the solution. If a negative potential with respect to the potential of zero charge is applied, then positive ions are attracted.

The most important issue related with this potential is that it defines the condition for the adsorption and desorption. A shift in this value leads to a increase or decrease ion adsorption. These changes will be appreciated in the experimental results of chapter 4.

2.3 Optical deflection sensor.

2.3.1 Microcantilever

In order to measure the surface stress due to the electrochemical processes on the microcantilever, we buy the Mikromash CSC12 (tipless without coating) which is a silicon-made microcantilever. In figure 2.10 we see its dimension, which defines its mechanical properties: 10 kHz resonance frequency and a 0.03 N/m spring constant. This allows us to perform reliable surface stress measurements.

The gold coating process is realized in two steps: first, 2nm of titanium (Ti) are evaporated and then, without breaking vacuum, 100nm of gold are thermally evaporated. The pressure during the evaporation is on the order of 10^{-7} Torr. Ti is used as an adhesive between the silicon and the gold. At the end of the evaporation process we obtain a polycrystal gold surface on one side of the silicon microcantilever. This polycrystalline gold show a predominance of Au(111) [29] . Under these conditions the thiolated DNA monolayers can grow on the microcantilever's gold surface.

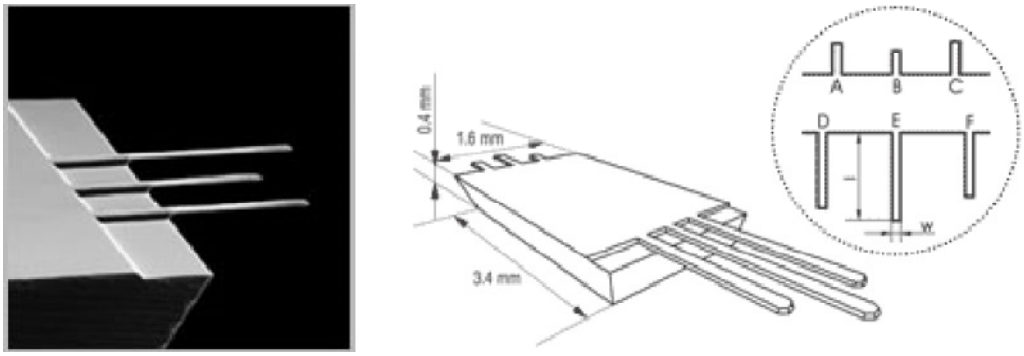

Figure 2.10: Microcantilever's SEM image and dimensions: Mikromash CSC12 (tipless without Al) [46]

We work the cantilever sensor in the static mode. In order to measure changes in surfaces stress**,** the optical beam deflection technique is used [43]. The laser light is reflected in the gold-coated front side of the cantilever (figure 2.11). The reflected beam is detected by a differential position sensitive photo detector (PSD) [44].

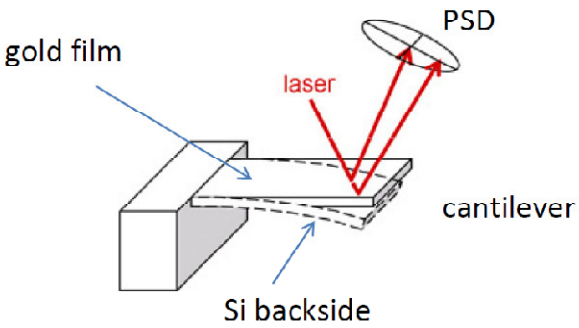

Figure 2.11: Optical beam deflection technique schematic.

This mode of operation is also used in atomic force microscope (AFM) [45]. Detailed description of the hardware , the calibration, and sensitivity can be found in the work by Tabard-Cossa and Monga [29, 46].

2.3.2 Surface stress calculation

From [29, 46] we use the following formulae (derived from Stoney's equation [47]) in order to calculate the surface stress on the gold-coated cantilever. The first equation establishes a relationship between the real deflection (in nm) and the voltage sensing in the PSD.

$$\Delta z = C_{cal}\Delta S \qquad \textbf{2.2}$$

In equation 2.2: Δz is the cantilever deflection change, C_{cal} is the calibration constant and ΔS is the voltage change on the PSD. Determination of C_{cal} is performed according to [29, 46] using interferometric calibration.

Equation 2.3 is used to calculate the surface stress change ($\Delta\sigma$).

$$\Delta\sigma = \frac{4}{3(1-\upsilon)} * \frac{l}{wt} k_{rect}\Delta z \qquad \textbf{2.3}$$

where υ, l, w, t and k_{rect} are the Poisson's ratio, length, width, thickness and spring constant of the microcantilever, respectively. The constant 4/3 is due to the fact that the bending comes from a uniform surface stress, as opposed to a concentrated load applied at the tip. We measure the changes of surface stress rather than the absolute surface stress.

3: Self-assembly of organothiol-monolayers and surface stress induced by adsorption on gold surfaces.

This chapter is a theoretical introduction about our chemical structure (organothiol-monolayers) and about the physical principles of our transducer (surface stress induced by adsorption).

The immobilization of biomolecules on surfaces is of great interest for many medical and bioanalytical applications such as biosensors. A wide range of procedures is available for the modification of surfaces to achieve immobilization.

Immobilization by self-assembled monolayers (SAMs) is an easy and well-studied method to created biomolecule (DNA) monolayers. SAMs offer flexibility and the capability to insert modifications on a molecular level. Therefore, the use of SAMs is increasing for various fields of research. This chapter is focused on the properties of thiol-DNA monolayers.

Biochemical sensing for bioanalytical methods requires the attachment of biomolecules to a suitable surface. The role of these sensing molecules is to provide chemical specificity and selectivity as well as enabling signal transduction. Procedures range from simple physisorption to Langmuir–Blodget films [48] to direct and covalent immobilization of biomolecules on surfaces using self-assembled monolayers or coupling to polymers. The formation of ordered and orientated monomolecular layers by spontaneous adsorption from a diluted solution is called self-assembling; the respective layers are called self-assembled monolayers (SAM) or self-organized

monolayers [49]. The selection of the substrate for immobilization depends on the application. For example, SAMs are often used for the development of biosensors with electrochemical, piezoelectric, or optical detectors. Glass and silica are typical materials for optical sensors, whereas gold is preferred for electrochemical sensors because of its inert properties. The combination of thiol compounds and gold is one of the best established SAM combinations. Details are found in [48-50]

3.1 Organothiol-SAM formation

Organothiol monolayers are based on the strong adsorption of thiols (R-SH) onto metal surfaces. Although thiols can strongly bond with different metals like gold, platinum, silver or copper, gold is the substrate of choice due to its inert properties and for its well-defined crystal structure. Organothiols consisting of an organic molecule with attached SH-group are well suited to fabricating structurally well defined adlayers of monolayer thickness on gold substrates using a simple preparation procedure [51-52]. The synthesis of organothiol-SAMs on gold strongly depends on the cleanliness and the crystallographic state of gold. The preferable gold surface state for the synthesis of organothiol is Au(111) [53].

There are different methods to analyze and characterize SAMs. We will list the most used techniques taken from [54]: Scanning tunnelling microscopy (STM), contact angle measurements, infrared (IR) spectroscopy, X-ray photoelectron spectroscopy (XPS), near-edge X-ray absorption fine structure spectroscopy (NEXAFS), X-ray diffraction (XRD), diffraction of low-energy electrons (LEED), helium atom scattering (HAS), surface plasmon resonance spectroscopy (SPR), and theoretical calculations of organic surfaces exposed by SAMs.

Among these characterization techniques, the electrochemical technique is more than a characterization technique, since it also changes the structure of the SAM system. In combination with other characterization techniques such STM, it is possible to analyze and characterize an important other property: defect density of the SAM monolayer. To calculate the surface defect density of the monolayer, the ferrocenethiol method has been shown to provide a reliable measurement [55].

3.1.1 Structure of thiol functional group

The binding or functional group of thiols is –SH, the sulfhydryl group, bounded to a tetrahedral carbon. Thiols are weak acids and react with bases to loose a proton [56]. Because of the low polarity of the S-H bond, thiols show little association by hydrogen bonding. Sulfur and carbon have a small difference in electronegativity, so the bond is non polar. [57].

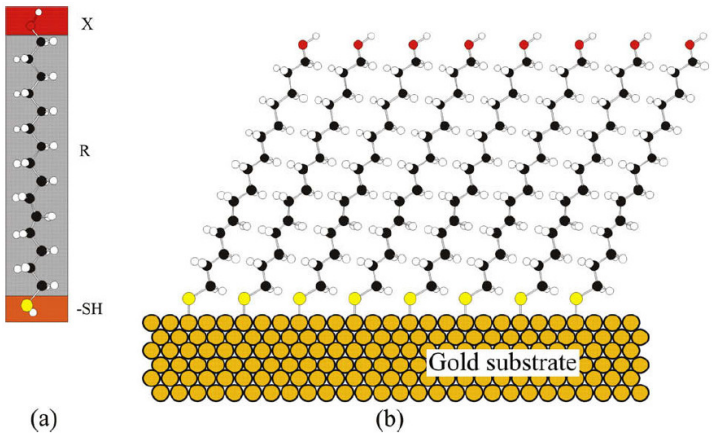

Figure 3.1: A thiol functional group on gold from [54].

The thiol functional group has three basic elements shown in figure 3.1: The anchor group (SH unit), the coupling unit R (in this case an alkyl group), and the

terminal function X (in figure 3.1 OH). The representation of the entire thiol group is SH-R-X. The anchor group (SH unit) is responsible for the chemical link with the gold surface. Gold and sulfur create a solid bond that gives stability to the organothiol-SAM [54].

As we will see later, our experiments use a low thiolated DNA surface density (<30%). Chapter 4.4 will describe how this is achieved.

3.2 Surface stress

Surface stress is a phenomenon related to the creation of a surface in a solid [58]. To understand the surface stress of an adsorbate-covered surface, we will begin by exploring the surface stress of clean surfaces.

3.2.1 The origin of surface stress

From the atomistic point of view, the coordination of atoms on surfaces is different from that inside the bulk. As a result, the charge density in the vicinity of the surface is redistributed.This manifest itself as a change in the chemical bonding and the equilibrium interatomic distances at the surface are different from that inside the bulk. The smaller surface bond length (bond relaxation) generally leads to a tensile surface stress [59].

Figure 3.2 shows a simple model of the charge redistribution which explains the tensile surface stress on metals. Figure 3.2a shows the model of the charge distribution inside a bulk in a truncated bulk structure. Figure 3.2b shows the model of charge redistribution when a surface is created. The surface atoms have no neighbour atoms on

top; to redistribute charges, surface atoms move close together. As a result, clean metals have a tensile surface stress on their surfaces [60].

3.2.2 Surface stress at adsorbate-covered solids

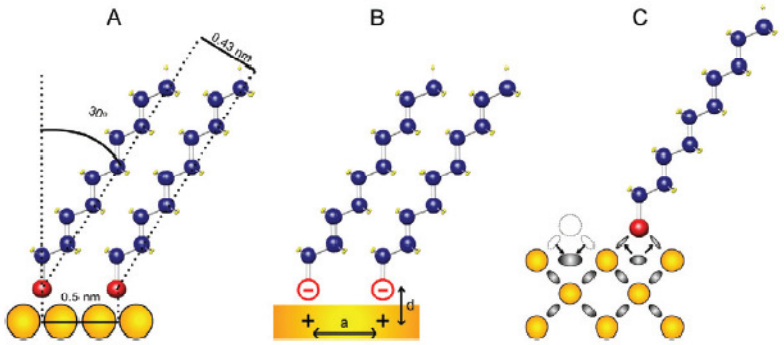

Figure 3.2: Alkanethiol molecules adsorbed onto gold surfaces: A) Lennard-Jones interactions between adjacent alkanethiol molecules. A molecular tilt reduces the inter-chain distances. B) Electrostatic repulsion between adjacent Au+S- bonds generates compressive surface stress. The intermolecule distance, a, is the distance between adjacent thiol headgroups. In SAMs, the positive and negative charges appear to be separated by a distance d. C) Electronic charge distribution near the gold surface modified by adsorption of alkanethiol molecules. This new distribution alters the local electron density, resulting in changes in surface stress [11].

The presence of atoms or molecules chemisorbed on the surface of a metal leads to different bonding configuration and different physical properties. To explain surface stress in clean surfaces, it is essential to understand the redistribution of bonding and/or antibonding charge at the surface of the bulk. In the case of adsorbate-covered solids, this criterion is still essential but additionally we have to take into account the neighbouring adsorbate atoms. This last effect becomes more significant when the adsorbate coverage is higher [59, 61]. Most of the knowledge about surface stress on adsorbate-covered surfaces comes from experiments using the cantilever bending

method [62-63]. The cantilever bending method in combination with electrochemical methods are the basic tools used in our DNA hybridization sensor. The adsorption and desorption of chloride ions (Cl^-) is stimulated electrochemically. The experimental details are exposed in the next chapter.

3.2.3 Cantilever bending method.

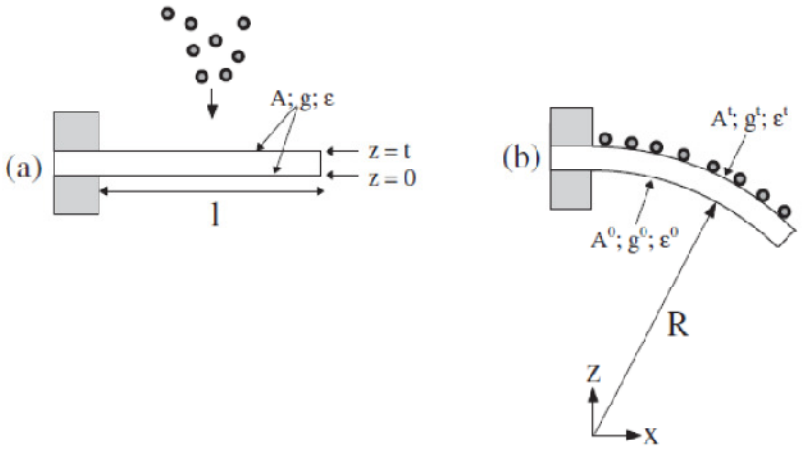

Figure 3.3: Adsorbate-induced surface stress measurement by bending cantilever method [64]

Figure 3.3 shows the bending cantilever method. The surface stress before adsorption (figure 3.3a) is assumed to be the same on both sides. The bending moment is zero at this point. As figure 3.3b shows, a chemisorption of any kind that takes place only on one side of the cantilever creates a surface stress difference $\Delta g = g^t - g^0$. This difference induces a bending moment that deforms the cantilever. The quantitative analysis of this deformation requires some assumptions to keep it as simple as possible.

These assumptions are:

1. The bending of the cantilever is very small, keeping constant the coordinates during the bending process.
2. The length of the cantilever l is large compared with the width , which is large with respect to its thickness, t.
3. The surface region is made of several atomic layers and its thickness is negligible in comparison with t. The component of the stress which acts in the x direction (i.e. g_{xx}^{0} and g_{xx}^{d}) determines the bending in the *x-y* plane.
4. The holder does not exert any forces on the cantilever.

The bending curve is a section of a circle in the *x–y* plane as shown in figure 3.3b, since the bending moment, which is induced by the surface stress, is constant along the *x* axis. With these assumptions, we arrive at Stoney's equation:

$$g_{xx}^{d} - g_{xx}^{0} = Yt^{2} / ((1- \nu) 6R) \qquad \textbf{3.1}$$

Where Y is the Young modulus and ν is the Poisson number. These terms have to be chosen according to the orientation of the cantilever. g_{xx}^{0} is the component of the surface stress in the *x* direction at the back side of the cantilever (figure 3.4b, *t*=0) and g_{xx}^{d} is the surface stress in the *x* direction at thickness equal to d (*t*=d). Finally, R is the radius used in the plane *x-y* as a reference for the deflection curve (figure 3.3b) The details of the mathematical deduction of Stoney's equation can be taken from [47].

4: Characterization of DNA functionalization with electrochemical protocols.

In this chapter, we will describe in detail our new functionalization protocol and the experimental results related to the biosensor probe's functionalization. A reliable technique for the functionalization of thiolated ssDNA (probe-DNA) allows the probe to have consistency and repeatability when hybridized. Two functionalization protocols are compared: a) the single step DNA functionalization protocol (traditional protocol) and b) our new multistep DNA functionalization protocol. The protocol b) gives a controllable surface coverage, and is the main topic of this chapter.

The traditional single step DNA functionalization protocol leads to irreproducible results and will be discussed in section 4.4. This is a surprising discovery related to the fact that incubation time is not a good control parameter to achieve a certain molecular coverage of a surface by self assembly.

4.1 Experimental procedure:

Our method consists of the following steps:

DNA samples preparation: 13-mer and 25-mer oligonucleotides (synthetic single strand DNA) are used [65]. The probe oligonucleotides "probe DNA" has a thiol-modification at the 5' end so as to covalently bond to the gold surface. TRIS-HCl 10mM NaCl 50mM buffer (TN buffer), pH=7.4 +/- 0.1, is used for the oligonucleotide preparation and all measurements. The probe DNA is desalted and the protecting group associated with the sulfur was removed using 0.1M DTT. Excess DTT from the probe DNA solution is

removed by column filtration right before experiments (3 or 4 times) using illustra NAP 5 column from GE Healthcare [66]. We have found that even trace amounts of DTT competitively bind to the Au surface, displacing thiolated DNA and lead to a reduction of the observable stress signal. Approximately 3µM of ssDNA in 100µl are usually obtained. All samples are prepared and used the same day to avoid effects from the oxidation of unprotected thiol and DNA bases.

Cantilever preparation: we evaporate titanium (2nm) and gold (100nm) on one side of a Mikromash CSC12 tipless silicon microcantilever [26]. We cover the the cantilever base with Eccobond 286 epoxy glue [28] to limit the area of the working electrode to the cantilever (chapter 2). Immediately before the experiment the microcantilever is electrochemically cleaned by cyclic voltammetry (CV) in $KClO_4$ (50mM) between -800 to 1300mV. The $KClO_4$ solution was purged with argon gas for 30 minutes before applying the CV. A sweep rate of a 20 mV/s is used.

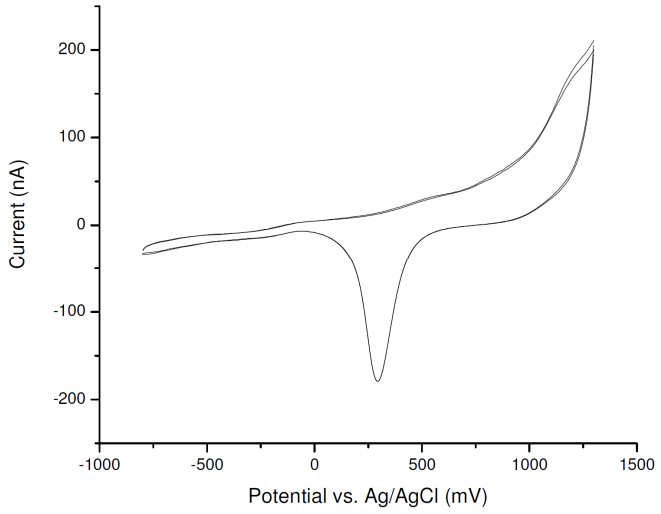

Fig 4.1: Cyclic voltammogram of gold surface cleaning with 50mM $KClO_4$ (used in Exp4 –figure4.11)

Functionalization: the microcantilever is then incubated in thiol-modified ssDNA (3µM) with a 0mV holding potential. After this functionalization step, the cantilever is mounted in the cell.

Characterization process:

a) Square potential experiment: we apply a periodic square potential +/-200mV, with a period of 10min after each incubation step described above. This protocol is a periodic adaptation of chronoamperometry [36, 37] which uses faster cyclic periods. The potential range is chosen to correspond to limited anion adsorption (-200mV) to significant anion adsorption (+200mV) (figure 4.2) [21] due to the present of Cl^- ions of the TN buffer (Tris-HCl 10mM NaCl 50 mM). Anion adsorption is observed in induce compressive stress changes in gold-coated microcantilevers (Godin et al 2010 [11]). The deflection induced by modulations of the surface stress is measured by the laser deflection method [43].

b) To characterize surface stress change vs. potential with respect to Ag/AgCl, we use a cyclic voltammetry from -800 mV to +700 mV and scan rate of 20 mV/sec

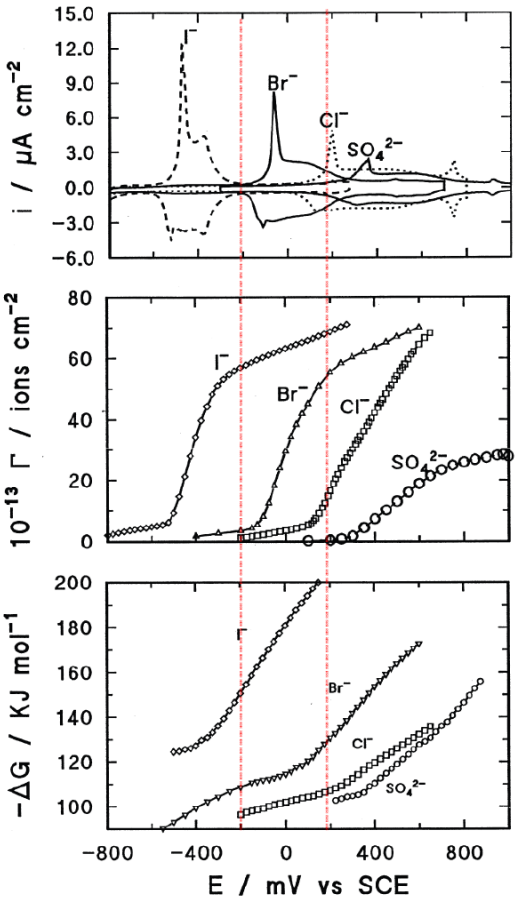

c) mV/sec.

Figure 4.2: Adsorption of ions. J Lipkowski et al. [21]. Top: current density vs. potential (vs. SCE). Center: Surface concentration of ions vs. potential (vs. SCE). Bottom: Strength of ionic adsorption vs. potential (vs. SCE). Red lines: +/-200mV vs. Ag/AgCl

Figure 4.2 shows adsorption at Au (111) electrode with Br^-, Cl^-, and SO_4^{2-} [21]. SO_4^{2-} has similar adsorption rate as phosphate ion (PO_3^{2-}) [67]. In our system, we have Cl^- from buffer and phosphate ions from DNA back bone. The origin of the cantilever deflection is competitive adsorption between Cl^- and phosphate (SO_4^-2) ions.

4.2 Response of DNA under electrochemical stimulation

To understand DNA sensing, we performed different experiments using electrochemical protocols (chapter 2) such as cyclic voltammetry and square wave potential on clean gold cantilevers, ssDNA (probe only) and dsDNA (target hybridized with probe) (chapter 2). In addition, a fluorescence quenching experiment [68] was used to observe the conformational state changes of the ssDNA under +/- 200 mV of electrochemical square potential stimulation (potential vs. Ag/AgCl).

Remember that the electrochemical induced adsorption and desorption of ions on the cantilever's gold surface, are the main factors that produce surface stress changes on the gold-coated cantilever as we will show in this chapter [11].

In Figure 4.3, cyclic voltammetry (-800 mV, +700 mV, sweep rate: 20mV/s) is applied to the probe and the surface stress change is measured by optical deflection sensing [43]. One oxidation cycle is shown (increasing part: -800 mV to +700 mV). Over this wide range, the differences in surface stress change are significant.

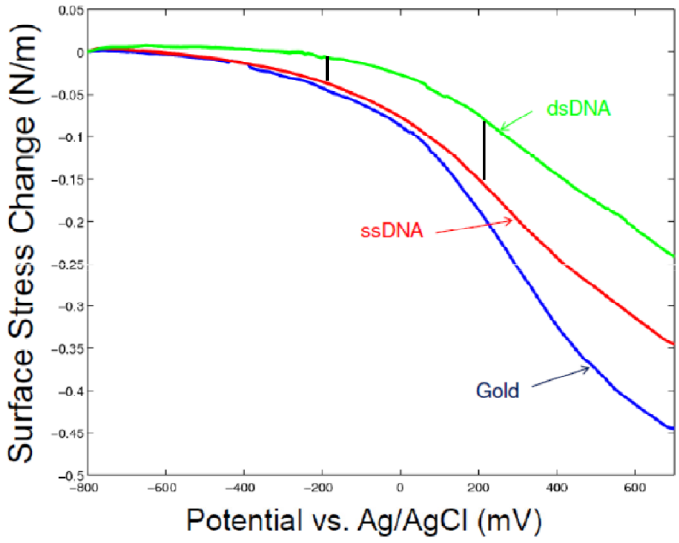

Fig. 4.3: Surface stress change of cantilever under electrochemical stimulus: bare gold (blue), ssDNA (red), and dsDNA (green) coated cantilevers (rate: 20mV/sec, [NaCl] = 50mM). [Data by Y. Nagai]

An important feature of a biosensor (hybridization detector) is to maximize the differences in surfaces stress changes between gold-only, ssDNA and dsDNA over the functionalized cantilevers [69].

In figure 4.3, the bare gold stress change is produced by Cl^- adsorption on the gold surface. Both ssDNA and dsDNA stresses are smaller than the bare gold stress because ssDNA and dsDNA reduce Cl^- adsorption on the gold surface as a result of the strand DNA blocking Cl^- ions. The signal arises from a change in ions adsorbed at the gold-coated cantilever surface [69]. Figure 4.3 shows the differences in surface stress change; in particular the different behaviour between ssDNA and dsDNA for a potential switching from -200mV to +200mV is about 100mN/m, a little smaller than the stress change on bare gold in the same potential window.

4.2.1 Response to square wave potential vs. Ag/AgCl

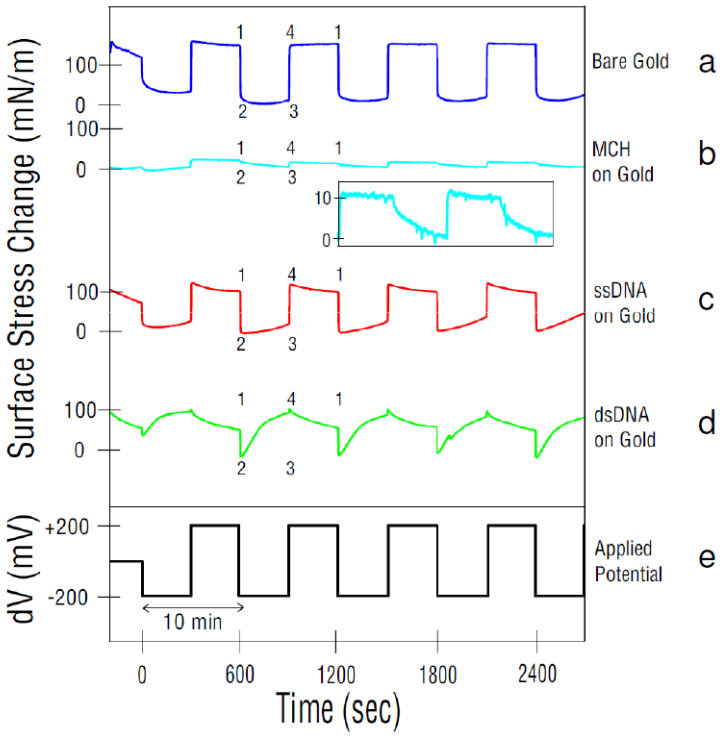

Figure 4.4: Surface stress response ("stress grams") to square wave potential.

Electrolyte: [NaCl] = 50mM (Cl^- as adsorbate and Na^+ ions).

With an electrochemical square wave potential of +/-200mV vs. Ag/AgCl and a period of 5 minutes applied to the ssDNA functionalized substrate, we observe the expected differences (~100mN/m) in stress and discovered significant differences in the surface stress patterns between ssDNA and dsDNA. Reproducibility of this result demonstrates a reliable hybridization detector, the aim of our experiments. An important experimental observation, to be discussed in 4.3 and 4.4, is that repeatability of our biosensor is mainly depended on the ssDNA surface coverage which needs to be carefully controlled. We will describe a reliable protocol to achieve this.

Figure 4.4 shows four different experiments that use the same electrochemical input (+/-200mV, 10min period). These experiments are:

a) The bare gold experiment.

b) The mercaptohexanol (MCH) experiment.

c) The single stranded DNA (ssDNA) on gold experiment

d) The double stranded DNA (dsDNA) on gold experiment.

MCH experiment (b) The MCH molecules are small, bind strongly to gold, forming a compact, defect free, monolayer and thus blocks the adsorption and desorption of ions on the gold surface. We observe that the amplitude of the surface stress for the MCH-coated cantilever was reduced by 93% (13 mN/m) of that observed for cleaned bare gold (167 mN/m) [69]. This experiment proves that the surface stress change depends on the exposed area and ion adsorption. In the bare gold experiment (a), the adsorption and desorption process of Cl^- is possible, the observed surface stress change is the largest observable (about 0.15N/m).

4.2.2 The fluorescence quenching experiment

In the square wave potential vs. Ag/AgCl experiment, we infer that dsDNA and ssDNA have different dynamic properties when the +/-200 mV (potential vs. Ag/AgCl) is applied. In the case of -200 mV potential, the strands of DNA tries to stand up and in the case of +200 mV the strands of DNA tries to lay them down. This is one of the reasons why there are noticeable differences in the surface stress change between ssDNA and dsDNA.

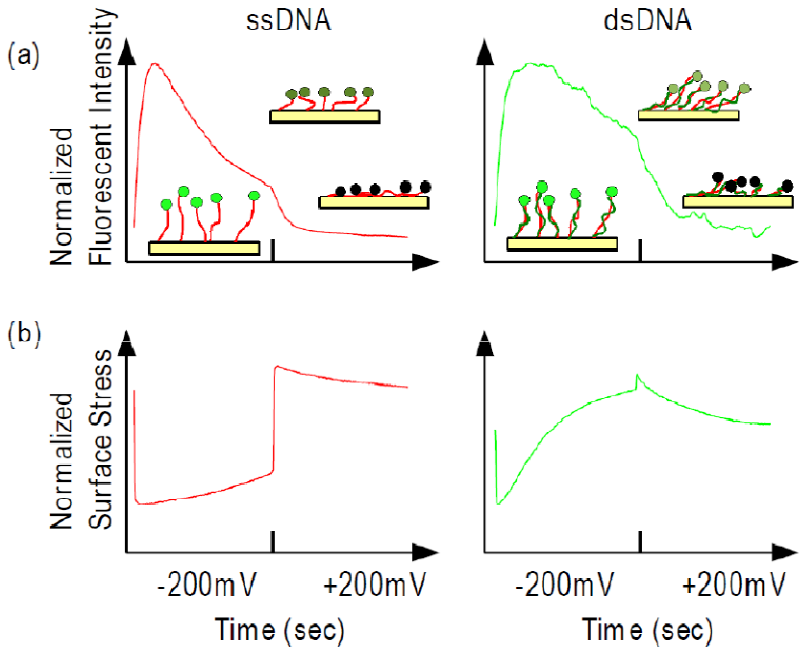

Figure 4.5: The fluorescence quenching experiment. Data obtained by Y. Nagai.

In order to experimentally demonstrate this, we performed the fluorescence quenching experiment. In this experiment a dye is attached to the 3' end of the ssDNA. We use the molecule Alexa Fluor 488 [70] as fluorescence dye. Note that U. Rant et al did a similar experiment but with a smaller time period (10 sec) [71]. When the dye is close to the gold surface, a quenching effect is produce and the fluorescent intensity decay dramatically. Because of the negative charge of the DNA backbone (phosphate backbone), the ssDNA is attracted by the +200 mV potencial vs. Ag/AgCl on the gold surface and its proximity to the gold surface quench the fluorescence of the dye. In figure 4.5 show two different shape or states: when the dye is far from the gold surface (-200 mV) and when the quenching effects happen at +200 mV. This experiment proves that the signal observed for ssDNA change its position with respect to the gold surface (up and down movements represented in cartoons of figure 4.5).

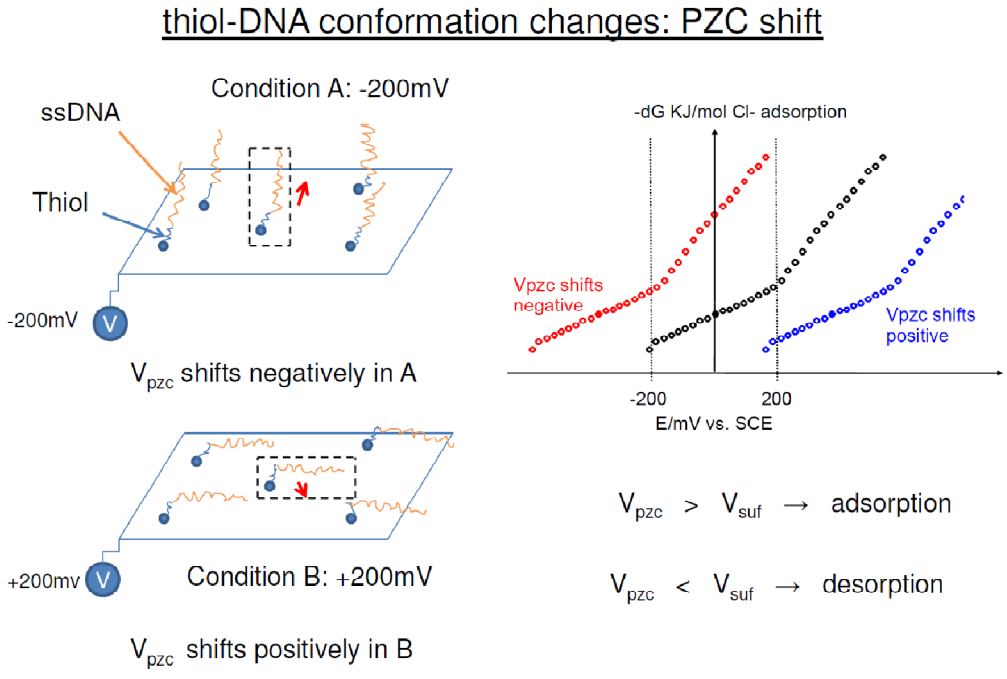

Figure 4.6: Effect of thiol-DNA conformation and V_{pzc} shifts on adsorption and desorption. V_{suf} is the surface potential of the gold-coated cantilever. (inset based on J Lipkowski [21]).

Fig. 4.6 shows how a V_{pzc} shift varies the extent of adsorption (inset, figure 4.6) [21]. The electrical environment at -200mV vs. Ag/AgCl produces a negative V_{pzc} shift, increasing adsorption and thus compressive stress, similar to the clean gold case. On the other hand, at +200mV vs. Ag/AgCl, a positive V_{pzc} shift is produced, decreasing adsorption and inducing desorption. The pattern of surface stress in fig. 4.4 (ssDNA: red) is a result of these changes in adsorption and desorption. In the -200mV vs. Ag/AgCl state, the surface stress change goes from a less compressed state to a more compressed state due to more chloride ion adsorption (negative V_{pzc} shift). Similarly, at the +200mV state, the surface stress change goes from a more compressed state to a less compressed state which means chloride ion desorption (positive V_{pzc} shift).

The kinetics of the ssDNA and dsDNA due to their mechanical properties and the dipole moment present on the thiol link group of the probe-DNA change the extent of the adsorption in the chloride ions.

In the case of dsDNA, effects attributed to ssDNA are amplified and modified due to the double backbone, the larger persistent length (25 larger than ssDNA) [71], corresponding to a more solid, rod-like structure of dsDNA and corresponding changes in dynamics.

The quantitative calculation is more difficult due to the necessity of including the resultant dipole moment of the probe-DNA. This is a function of the DNA sequence (different base pairs have usually different dipole moments, see appendix C), the ssDNA backbone induced dipole moment and the counterions induced dipole moment [72]. Additionally, the permanent dipole moment presented on the DNA strand change with its conformation and direction [73].

4.3 DNA single step functionalization protocol

In the DNA single step functionalization method, the gold coated cantilever is immersed in a solution of probe ssDNA for a fixed amount of time, typically in the range of 5 minutes to 30 minutes. One constraint of the ssDNA single step functionalization protocol is that we do not know how the DNA functionalization process is evolving over this fixed time. We observe that statistical variations and surface conditions make the functionalization highly variable. As a result, it is hard to obtain reproducible and optimal ssDNA coverage on the cantilever by using this protocol. Single stranded DNA (ssDNA) surface coverage empirically shows a

distribution after fixed time single step incubation. We hypothesize that the reason for this variability is the surface conditions of gold associated with functionalized probe-ssDNA due to the variability in the orientation of DNA strands (ssDNA and dsDNA) affect the adsorption rate [69].

4.4 DNA Multistep functionalization protocol

In order to control the functionalization (or incubation) process, we developed a DNA multistep functionalization protocol (DNA-MSFP). This protocol is essentially a sequence of short single step functinalizations each followed by a characterization step. We used functionalization of 5 minutes, as this allows us to follow the evolution of the surface stress changes in the probe. The characterization step (explained in chapter 2) is an electrochemical protocol applied to the cantilever: a square wave potential is applied and the stress sensor response is measured. We incubate in periods of 5 minutes and after each period we characterize the result electrochemically by applying a square wave of +/-200 mV with a 10 minute period. At the same time we record the surface stress response of the cantilever. For the characterization process, we apply a minimum of 4 cycles (+/- 200 mV, 40 min of total recording).

4.4.1 Characterization of DNA Multistep Functionalization Protocol

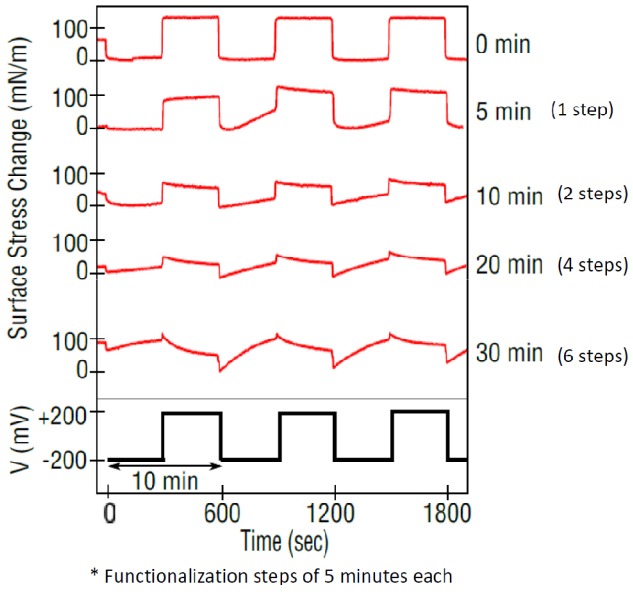

Figure 4.7: Characterization of the Multistep Functionalization Protocol.

Figure 4.7 shows the progressive change of the surface stress change response when several sequential DNA functionalization step are applied. A period of 5 minutes of functionalization is applied between each characterization step. In each step the cantilever is incubated for 5 minutes in a solution of thiolated ssDNA. The incubation process is made by submerging the gold-coated cantilever in a solution of 3μM thiolated ssDNA. After the 5min incubation the cantilever is placed again in the electrochemical cell for characterization. The response after 30 min (6 steps of 5 min incubation) is very similar to the response of dsDNA showed later in figure 4.9. An important challenge is thus to develop a criterion to achieve optimal ssDNA functionalization.

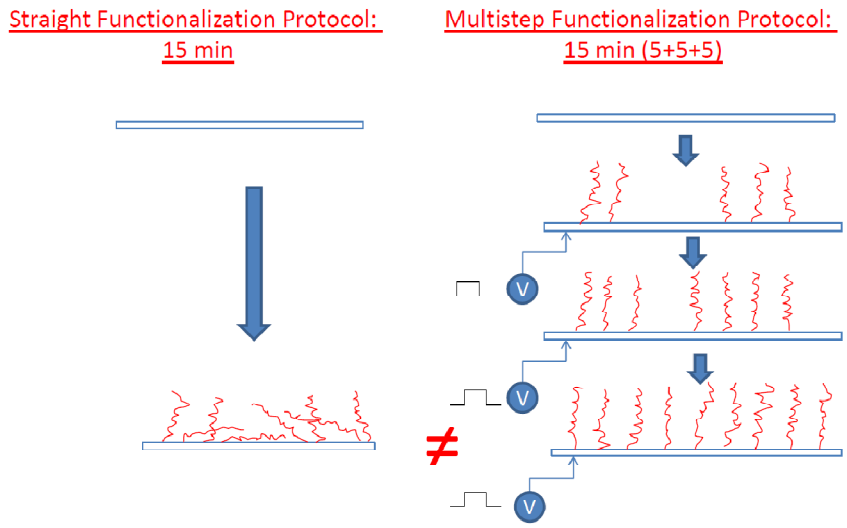

Figure 4.8: Interpretation of Single step Functionalization vs. Multistep Functionalization

In figure 4.8 we show our hypothesis of the differences between performing a direct functionalization and performing a sequential functionalization. Due to random collisions of thiolated-DNA to find an empty spot for functionalize with gold, the surface coverage using a direct functionalization protocol is highly variable and spatially non-uniform. The surface potential conditions can dramatically affect the beginning of the functionalization as we will observe in section 4.4.3.

We hypothesize that the electrochemical-induced dynamic periodic motion, reorient the DNA strands each time that a characterization process is applied and exposes some free space between DNA strands for the new 5 minute functionalization period. As a result, we obtain a faster and, in particular, more homogeneous functionalization due to the free space created between the DNA strands due to each characterization step. Finally, the characterization process allows us to define a reproducible coverage to stop the functionalization at the optimal probe coverage.

The surface stress grams collected from the characterization step give us important information about the coverage and the evolution of the cantilever functionalization.

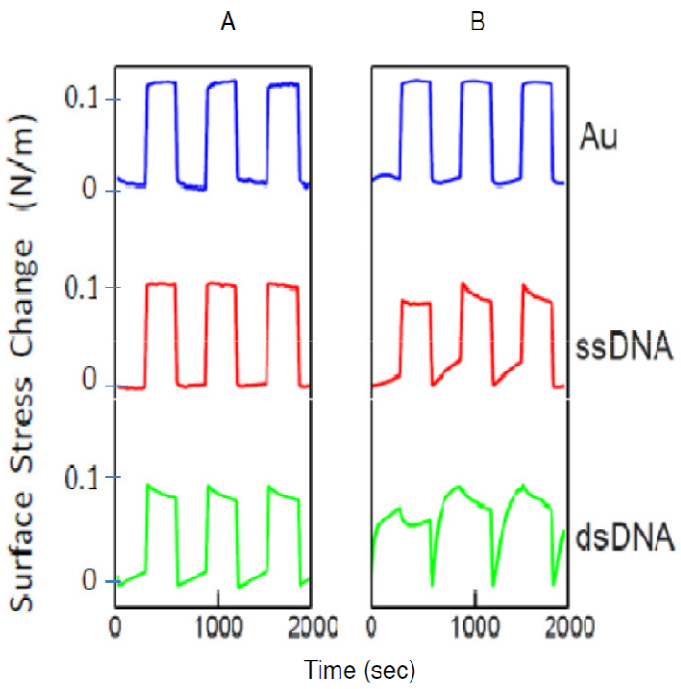

Figure 4.9: Variability of single time step functionalization protocol. A) 25-mer DNA, 15min of single step incubation B) 25-mer DNA, 15min of multistep incubation.

Figure 4.8 shows surface stress changes for different single step functionalization runs. Blue plots are the surface stress change from gold only cantilevers, red plots are from ssDNA on the cantilevers and green plots are from dsDNA on the gold cantilevers. 25-mer thiolated ssDNA was functionalized on the gold cantilever in a 15min single step in red (Fig. 4.8A) and then 25-mer target ssDNA was hybridized in green (Fig. 4.8A). In Fig. 4.8B, 25-mer thiolated ssDNA was functionalized sequentially on the gold cantilever with 5 min each. After every 5 min functionalization process, the gold cantilever with ssDNA was applied square potential +/-200mV with 10min period. The surface stress in fig (Fig. 4.8B) is from a multistep of

total three 5minute steps (for a total of 15min). DNA multistep functionalization processes. The green plot in fig. 4.8B) is from the dsDNA of 25-mer.

The major conclusion to be drawn from this data in figure 4.9 is that if the functionalization is not optimal, the characterization of the dsDNA can be confused with the characterization of the ssDNA at a higher surface density (fig. 4.8A green trace compared to fig. 4.8B red trace).

4.4.2 Surface Stress Change Evolution using Multistep Functionalization Protocol.

The aim of this section is to observe the evolution of the surface stress with time and to distinguish two well-differenciated periods: The fast functionalization of DNA (first steps of DNA-MSFP) and the approach to a saturated DNA coverage (latest steps in DNA-MSFP with many functionalization periods). From this point forward, we use only 25 mer DNA.

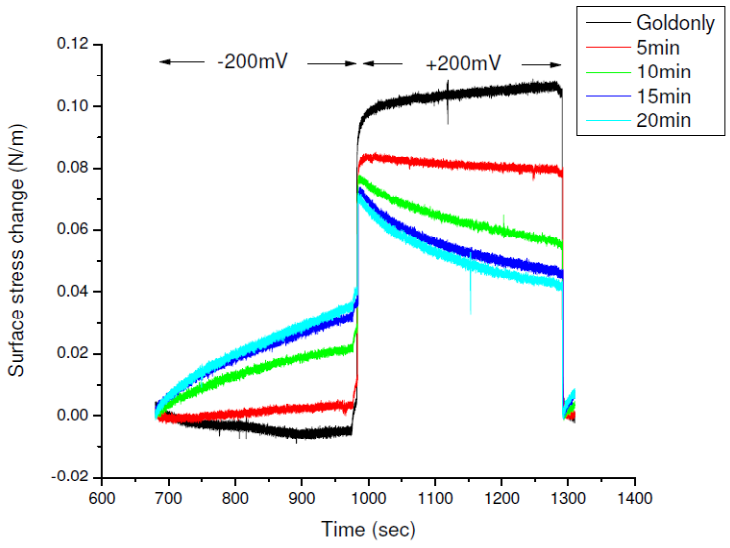

Figure 4.10: Evolution of Surface Stress Changes in DNA-MSFP for initial 4 incubation steps (total functionalization time: 0 to 20 min, solution: Tris-HCl 10 mM NaCl 50 mM, pH = 7.4).

The evolution of the surface stress changes at the beginning of DNA-MSFP is showed in Figure 4.10. It shows the first five steps: clean gold-only (0min), 5 min, 10 min, 15 min and 20 min total of DNA-MSFP. The maximum difference in surface stress change is obtained at the initial condition (gold-only, black). After this point, not only the magnitude but also the shape of the surface stress gram changes. The change in magnitude is a maximum between gold-only (0 min) and the first step of DNA-MSFP (5 min). This change in magnitude decreases with increased incubation time. In other words, the change in magnitude decreases while the number of DNA-MSFP steps increases. This reduction in magnitude is due to the reduction of gold surface available to ions after the previous five minutes of functionalization (figure 4.6).

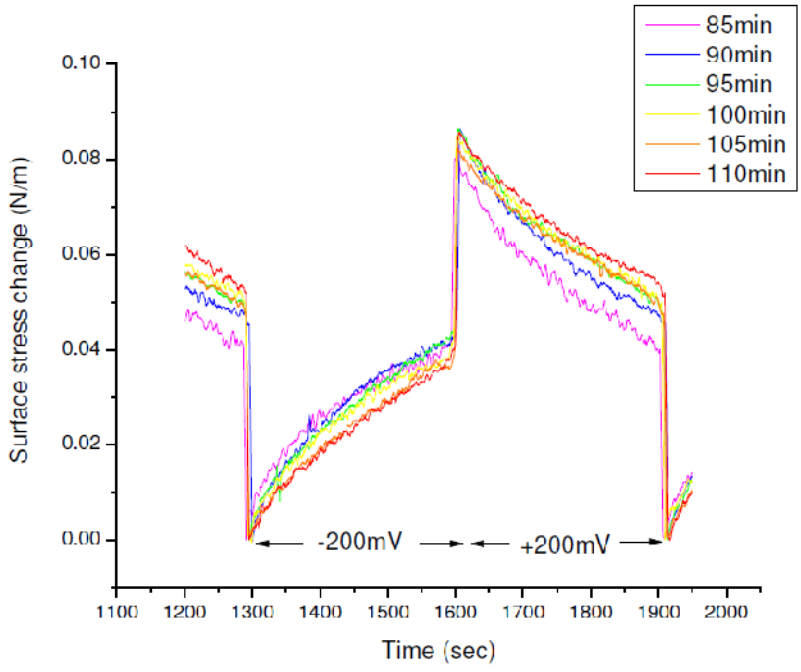

Figure 4.11: Evolution of Surface Stress Changes in DNA-MSFP for many functionalization steps (total functionalization time: 80 to 110 min, solution: solution: Tris-HCl 10 mM NaCl 50 mM, pH = 7.4).

In figure 4.11 we observe the result after many incubation steps when the ssDNA coverage is close saturation (or maximum coverage). The surface stress change is small, figure 11 shows stress grams for incubation steps 17 (85 min of total functionalization) up to step 22 (110 min of total functionalization). The small changes, compared with those observed after the first five steps, indicate that we are close to saturation coverage. At that saturation coverage the hybridization will be difficult to achieve due to steric hindrance. The reduced space between the probe ssDNA on the cantilever surface will not allow hybridization with the ssDNA target.

Note that on commercial gene chips, an optimal probe density is achieved by spacing the probe ssDNA with MCH. We cannot do this for our stress sensors as MCH strongly reduces the stress signal (fig 4.4).

We have a first important conclusion: We must not functionalize too close to the DNA saturation coverage because we will not get a noticeable change stress response upon hybridization. What is the optimal probe density that leads to the largest difference in signal, between ssDNA and hybridized, dsDNA?

4.4.3 Shape evolution of stress gram using DNA multistep functionalization

To answer this question we need to analyze the evolution of surface stress changes quantitatively. Our analysis is demonstrated by looking at one cycle of ten minutes of the stress gram from figure 4.9 and figure 4.10. At the point where the transition occurs (-200 mV jump to +200mV), we define two new values, - σ and σ. The value - σ is defined as the difference in surface stress change during the -200 mV stimulus (figure 4.12). The second value, σ, is defined as the maximum of surface stress

difference at the transition. We find that the dimensionless ratio -σ/σ is a parameter to follow the evolution of surface stress changes and associated ssDNA coverage.

Physically, the parameter -σ is the surface stress change induced by the presence of ssDNA on the gold-coated cantilever during the -200mV state. The value of -σ depends on the amount of ssDNA on the gold-coated cantilever. The parameter σ is the surface stress change induced at the moment of the transition from the -200mV state to the +200mV state. The value σ is used as a reference to normalize the changes of –σ.

Figure 4.12 shows the evolution of (-σ/σ) for 5 different cantilevers as a function of the total functionalization time (i.e. number of 5' functionalization steps). All the cantilevers were cleaned prior to these experiments using cyclic voltammetry (section 2.2.1).

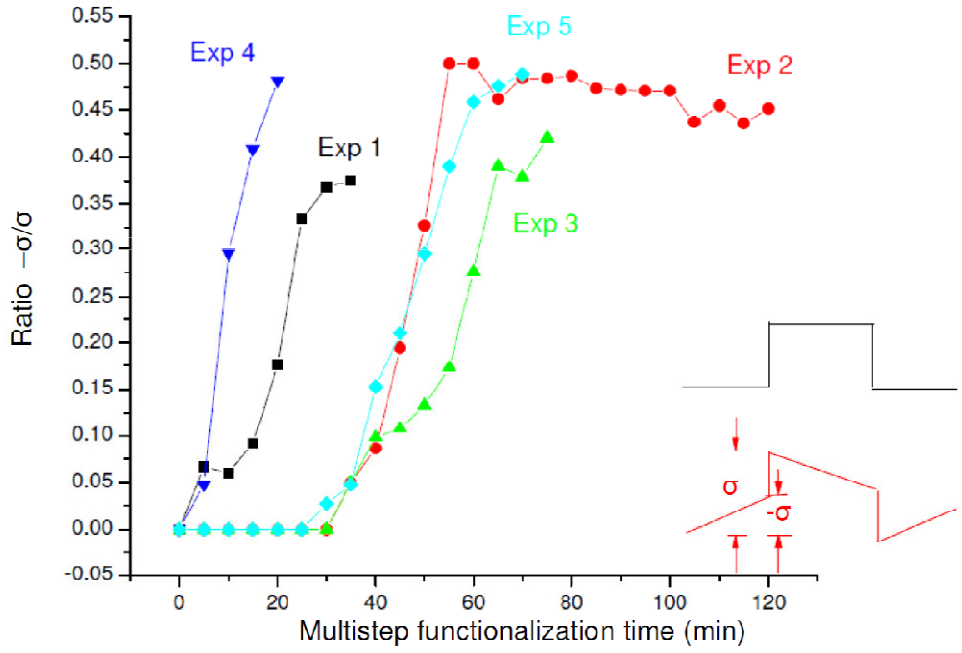

Figure 4.12: Shape evolution of the surface stress change response vs. Functionalization time

Figure 4.12 shows that incubating for n times 5 minutes leads to a distribution. After n functonalization steps, one does not always reach the same ratio $-\sigma/\sigma$ (and as we will later see same surface coverage). This is a further reflection of the stochastic nature of the self assembly process mentioned above. It shows also the general curve shape is very similar for all runs if a constant functionalization time offset is taken into account. This indicates that the fundamental ssDNA probe surface density and structure achieved is the the same, but different functionalization times are needed.

Figure 4.12 summarizes five experiments. The same ssDNA probe, prepared as described in section 4.1, was used within 24 hours of all experiment. All experiments were performed on the same day to reduce the variability present in aged ssDNA. We may attribute the onset of functionalization, as exhibited by a non-zero slope of $-\sigma/\sigma$ as primarily due to variations of the surface potential (V_{pzc}) [55]. To focus on the evolution of the $-\sigma/\sigma$ curve and to see when the saturation zone starts, we plot figure 4.13. In this figure we eliminate the transition time where there is no change in $-\sigma/\sigma$. In this plot all experiments 1-5 are thus aligned at the beginning of the functionalization.

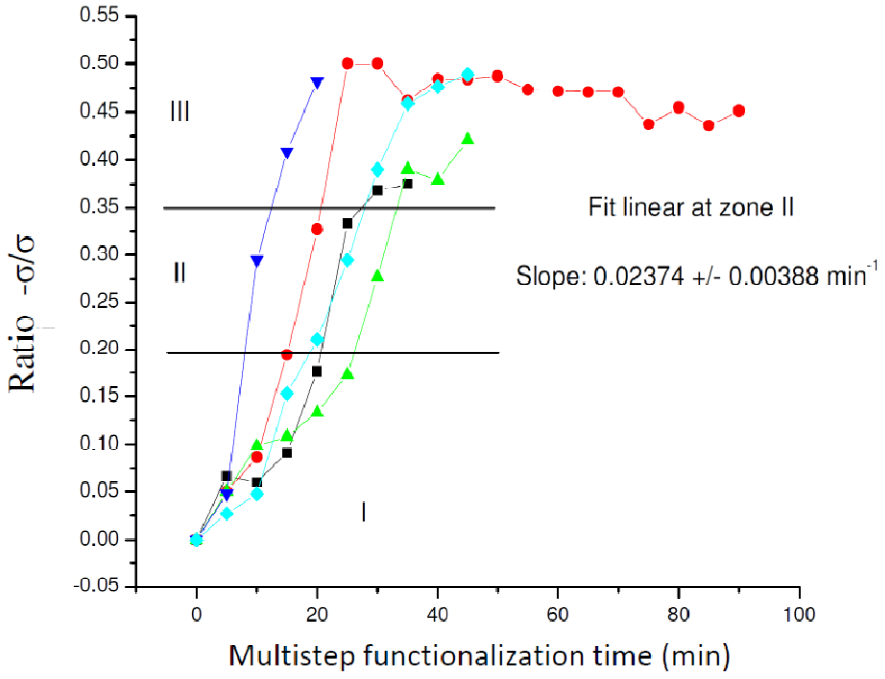

Figure 4.13: Shape evolution of the surface stress change response vs. Functionalization time (Omitting the delay time previous the beginning of the functionalization). Variability of slope in zone II: 16%.

We observe in fig 4.13 that the five experiments have a similar evolution between 0.2 and 0.35 (see average slope of all curves in figure 4.13). We establish three different zones:

a) Zone I: ($-\sigma/\sigma < 0.2$) where the DNA coverage is low.

b) Zone II: ($0.2 \leq -\sigma/\sigma \geq 0.35$) regime showing reliable DNA biosensor hybridization signal.

c) Zone III: ($-\sigma/\sigma \geq 0.35$) high DNA coverage, saturation regime, no difference between ssDNA and hybridized DNA observable.

A clear difference in the characteristic curve shape of ssDNA and dsDNA (fig 4.4, fig. 4.8A, and fig. 4.8C), is only observable when the value of $-\sigma/\sigma$ is in zone II. This

"shape criterion" or -σ/σ value can be used to achieve quantitative repeatability of the sensor response.

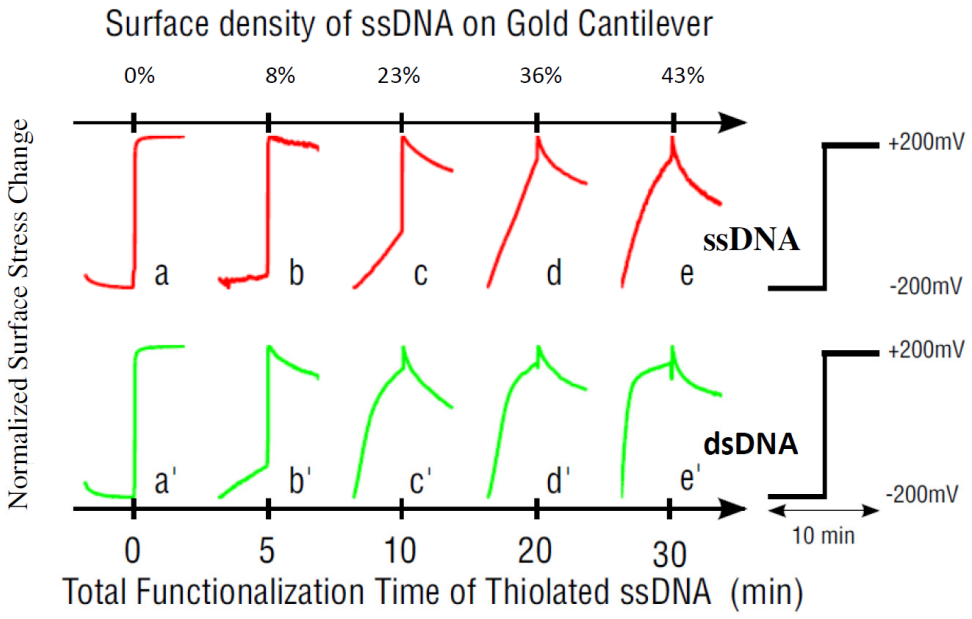

Figure 4.14 Hybridization patterns for different ssDNA surface densities.

Figure 4.14 shows the patterns in the stress gram as a result of the hybridization process for different values of ssDNA surface density. The surface density is measured by the ferrocenethiol method [55]. We see that the optimal value in this experiment to generate two noticeable different patterns between ssDNA and dsDNA is 20% of ssDNA surface density (-σ/σ=0.34). 10% of ssDNA surface density (-σ/σ=0.09) generates similar patterns for the ssDNA and dsDNA stress grams. If we are just 10% off the optimal probe density, our sensor cannot distinguish a signal - we speculate that this is one of the reasons for the large variability in stress values reported in the literature, the generally small measured stress and difficulty of many groups to reproduce data. The multi-step functionalization and characterization protocol described above is a simple method to circumvent this problem.

In summary, the ssDNA surface density values must be controlled to +/- 10% to generate optimal differences between ssDNA and dsDNA patterns. By means of the -σ/σ ratio, using a step-wise incubation subsequent characterization steps and aiming for -σ/σ=0.3 we can reproducibly achieve this in a controlled fashion.

4.4.4 Comparison of sensitivity between cyclic voltammograms and stress grams.

In the following we will compare the evolution of the cyclic voltammograms and plots of surface stress change as a function of the potential and as a function of the number of incubation steps (i.e. incubation time). In figure 4.15, we show this comparison. The two small graphs show the result for cyclic voltammograms for different functionalization times.

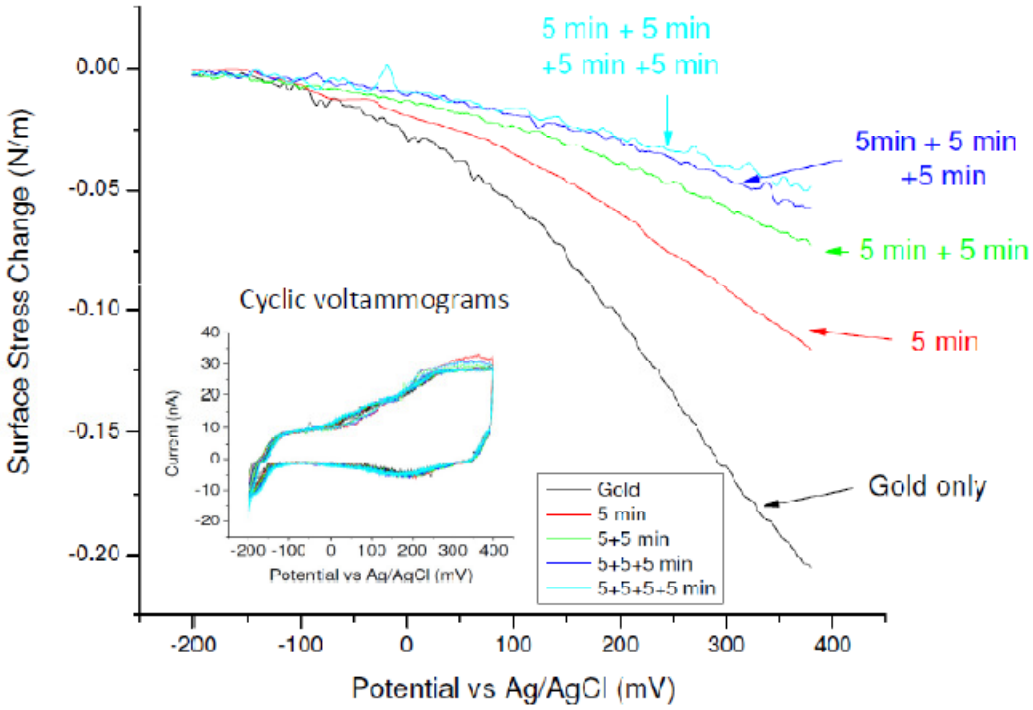

Figure: 4.15: Comparison of cyclic voltammograms with stress grams.

The following key observations are extracted from this graph (figure 4.15): First of all, it shows that the stress gram is more sensitive than the cyclic voltammogram. All the cyclic voltammograms are identical, independent of functionalization time (figure 4.16). In the case of the stress grams, we see noticeable differences. The surface stress change differences between consecutive steps are largest for the first few functionalization steps. The surface stress change difference is reduced with increased incubation time. The trend observed reveals a plateau where a high ssDNA coverage condition of the probe is given and no more surface stress change is presented, similar to observations of -σ/σ saturation.

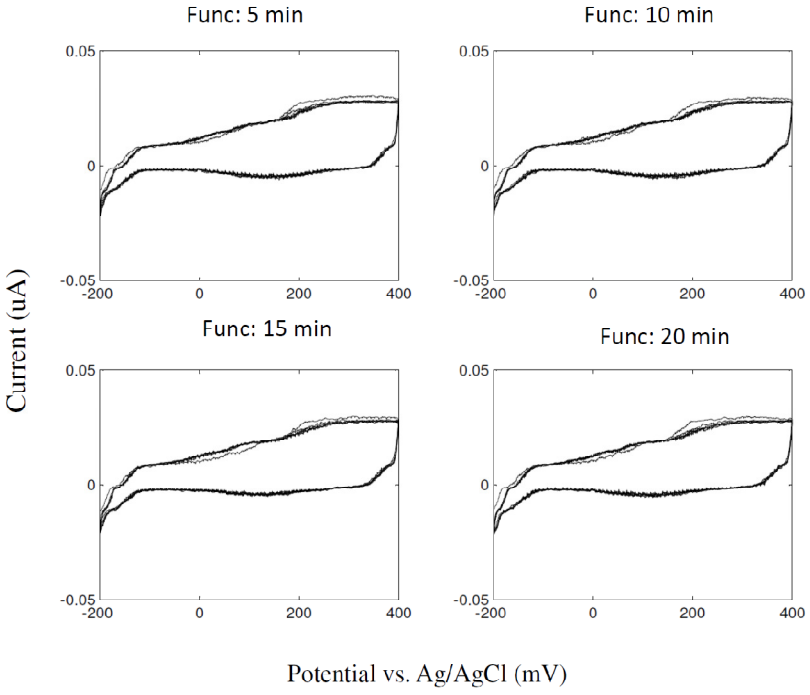

Figure 4.16 CVs at different functionalization times.

Incubation Time	CV area (Coulomb * E-6)
0 min	1.09 +/-0.01
05 min	1.12 +/-0.01
10 min	1.12 +/-0.01
15 min	1.12 +/-0.01
20 min	1.13 +/-0.01
25 min	1.12 +/-0.01
30 min	1.16 +/-0.01
35 min	1.15 +/-0.01
40 min	1.14 +/-0.01
45 min	1.15 +/-0.01

Table 4.1: Areas of CVs (A.sec) at different multistep functionalization times.

In summary, using the shape analysis (section 4.4.3) from the characterization step (figure 4.12) we can decide what values of the ratio $-\sigma/\sigma$ is optimal for our probes in order to maximize the sensitivity of our DNA sensors. The value of $-\sigma/\sigma$ is related to the coverage of ssDNA on the probe (fig. 4.14). This multistep functionalization process combined with characterization steps opens the possibility of several new experiments that will contribute to the understanding of the surface stress change phenomenon. It is also a very practical criterion that ensures the repeatability and reliability of cantilever based DNA sensors.

5: Conclusions and Outlook

5.1 Conclusions

In order to have repeatability in DNA surface stress change, we have to obtain similar surface conditions. A well defined functionalization process for the probe is required. As the previous chapter shows, it is possible to get the wrong readout because of low or high ssDNA coverage. By analyzing the shape of the coated cantilever response (stress gram), it is possible to achieve a maximum differentiation between ssDNA and dsDNA sensor response. This technique prevents misinterpretation of the DNA sensor response. Sequential functionalization gives us the possibility to control and verify optimal coverage, surprisingly incubating 20 minutes or in 4 steps of 5 minutes does not yield the same result. We attribute this to the fact that ssDNA is not stiff. It is possible to electrochemically stimulate ssDNA. This leads to rearrangement of the DNA strands, allowing access to unoccupied gold surface for other DNA strands to bond to the gold surface. Bottom line, we have developed a faster, controlled functionalization protocol.

This new DNA multistep functionalization protocol (section 4.4) is a feasible way to control the conditions of the ssDNA surface coverage of the probe on the gold-coated cantilever. In particular, measuring the dimensionless value $-\sigma/\sigma$ (figure 4.11) after each functionalization step can be used to decide to continue or not with the functionalization process, as it allows monitoring of probe coverage. The absolute value of $-\sigma/\sigma$ will depend of what class of biosensor or probe we are using. For example, we can use a hybridization detector, an aptamer or a mismatch binding detector. Each will probably have its own optimal $-\sigma/\sigma$ value. After a few systematic experiments we can

determine the range of values of -σ/σ where a particular probe-target system has an optimal response.

As demostrated, the ssDNA surface coverage of the cantilever is essential to obtain a reliable biosensor. In particular, maximum coverage is NOT optimal for hybridization detection via stress measurements. A coverage of 20%-30% is optimal. The development of DNA-MSFP is a crucial insight to build reliable biosensors. The coverage of ssDNA on the probe must be easily determined while the functionalization process is running.

Using a long period (10 min) square wave potential vs. Ag/AgCl (+/- 200mV) variations, we discovered noticeable qualitative differences between the stress gram of ssDNA and the stress gram of the dsDNA (figure 4.4). This protocol thus shows a reliable hybridization detector with a large S/N (signal to noise ratio). The period of ten minutes is long enough to follow all the processes involved, and study their kinetics including long relaxation times of the "standing up" and "lying down" phase of the strands of DNA (4.2.2). This platform can thus also be used to study such fundamental questions as the kinetics and dynamics of polyelectrolytes (such as DNA) near a solid surface.

5.2 Outlook

The DNA multistep functionalization protocol (DNA-MSFP) opens up new possible experiments. In the hybridization detection we keep many parameters constant: buffer (TRIS-HCl), electrolyte (NaCl), pH (7.2-7.5), ssDNA length (25mer,13mer) and

electrochemical settings (+/-200mV, 10 min period). The optimal value of -σ/σ depends on these parameters and is expected to be a function of them.

Once we obtain the range of values for -σ/σ, we are able to functionalize the probe (gold-coated cantilever) reproducibly and optimally for any new parameter. In a first crude approximation, the range of -σ/σ should be between the start of the saturation part (zone III – figure 4.12) and -σ/σ=0.

This protocol DNA-MSFP can be applied to other biosensor protocols such as melting detection, mismatch binding detectio, protein detection (aptamer). In the aptamer case, the size, the chemical and electrical properties of the proteins will play an important role that determines the values of -σ/σ for optimal probe coverage.

The DNA multistep functionalization protocol (DNA-MSFP) and characterization can be used as a general method to find the optimal conditions for the ssDNA cantilever's coverage. This thesis is a first step to have coherent DNA functionalization strategies for cantilever sensor. Well-defined, reproducible DNA coverage of the probe means reliable biosensor and repeatability of results, and is an important step from the lab to industrial applications.

Appendix A: ssDNA sample preparation and desalting method for thiolated ssDNA

Preparation of Oligonucleotides for Bonding to Gold Surface

- 25-mer oligonucleotides are shipped in powder form from Operon Biotechnologies.
- A 25-mer oligonucleotide (5'-[ThiSS]-TCGGATCTCACAGAATGGGATGGGC-3') has a molecular mass of 8075.5 g/mol.
- Each small well contains 40 μL of stock solution.
- 100 μM stock oligonucleotide solution is made with Tris-EDTA buffer (pH=7.4 from Sigma Aldrich [74]).

Cleavage of disulfide bond with DTT and desalting

1. Add stock oligonucleotide solution to well (40μL, 100μM of oligosolution).
2. Add the same volume of 0.1 M DTT solution and allow react for 30 min.
3. Using 1000 μL micropipette, add 400 μL of ethyl acetate for desalting process (breaking of disulfate bond).
4. Repeat step 3 three times.
5. While doing steps 5-8, also load NAP-5 column [33] with Tris-HCl 10mM, NaCl 50mM, pH=7.4 (TN buffer) 3 times.
6. As a final step to prepare the thiolated ssDNA sample, we use the nanodrop spectrophotometry using the software Nanodrop from Thermo Scientific [75] to calculate the concentration and quality of the thiolated ssDNA.

Appendix B: Electrochemical cell design and upgrade.

In order to perform future experiments that require a flow system and a small volume cell, we designed and built a new electrochemical cell. This cell will have new features that the electrochemical cell (chapter 2) used to perform the experiments shown in this thesis do not have.

An important application of microcantilevers is the detection of small quantities of biochemical molecules by mechanical cantilever deflection due to reactions on the gold coated and chemically functionalized surface. To achieve this goal, we designed and built a microcantilever sensor system allowing control and characterization of surface conditions, in-situ functionalization which can be dominant factors for signal generation and reproducibility in these systems [10].

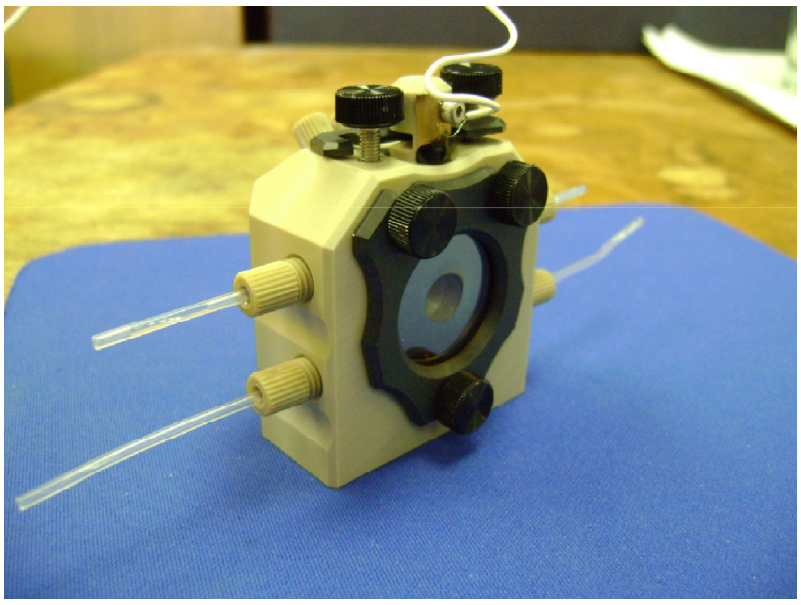

Figure B.1: Electrochemical cell with flow system. Constructed by Aleks Labuda.

The microcantilever system must perform stable electrochemical experiments, handle small volumes of electrochemical and biological solutions, and optically detect

deflections of the microcantilevers. This system has a modular configuration with a reliable flow system (to mix and exchange chemical and biochemical solutions). As a result, experiments using temperature control to monitor DNA melting and DNA hybridization can be performed. Additionally, the new design allows the cantilever to be submerged into the solution completely with an electrochemical isolation. This feature ensures controlled mixing of different chemicals inside the liquid cell.

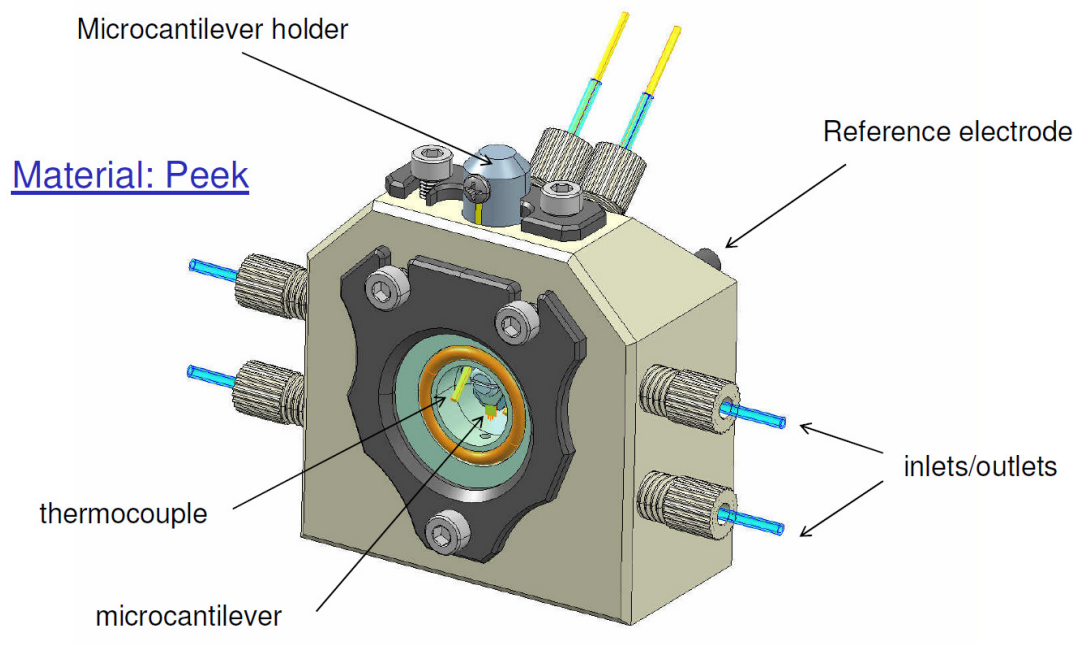

Figure B.2: Parts of the electrochemical cell.

Using this liquid cell we will work on DNA mismatch detection experiment changing the following variables: DNA length, salt concentration and electrochemical manipulation. Longer DNA samples have a higher melting temperature and each mismatch on a DNA sample reduces the melting temperature [76]. The ability to mix chemicals and to control temperature is crucial for developing a realistic biosensor system.

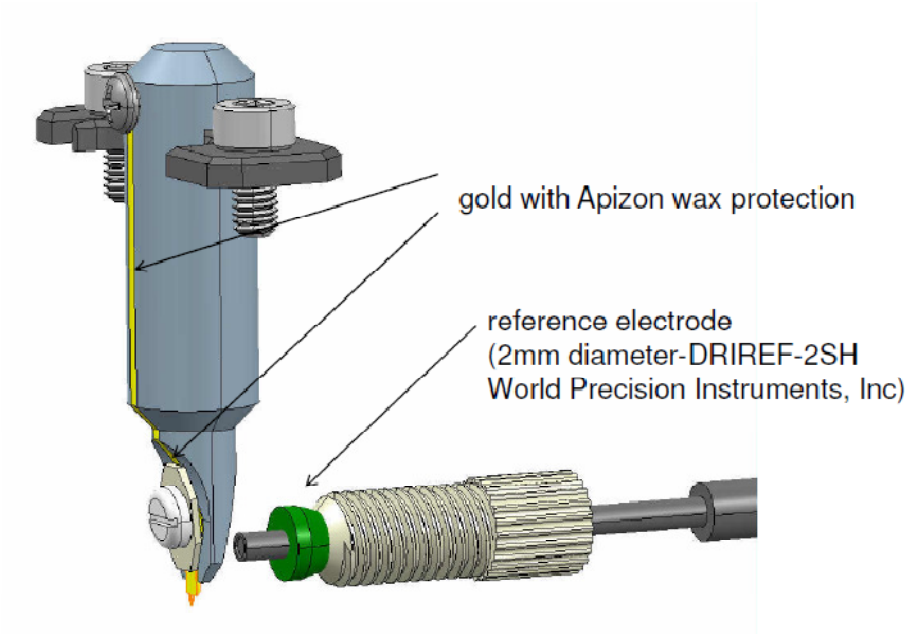

Figure B.3: Details of the cantilever's holder and the reference electrode.

The reason to use polyether ether ketone (PEEK) [77] instead of PTFE (Teflon) [78] is its hardness that makes PEEK to be easy to machine. The electrochemical properties of PEEK are similar to the PTFE. In order to machine a small cell with flow system, it is more reliable to use PEEK. The machining of the small connections for the tubing is more precise with PEEK.

The electrochemical cell has the following capabilities:

- Flow system is available.
- Liquid cell volume reduced (600 μL).
- Oxygen contamination reduced.
- Argon injection is available.
- Thermocouple is available.
- Larger counter electrode (CE) area (sputtered Au or Pt on front glass).

- No meniscus or variable meniscus.

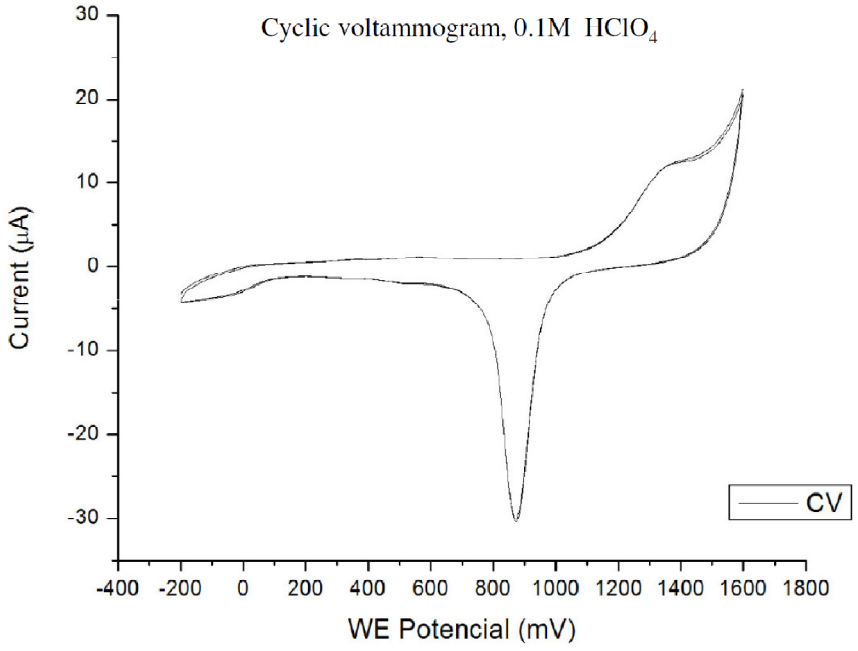

Figure B.4: WE surface cleaning CV using 0.1M $HClO_4$, scan rate: 20mV/s

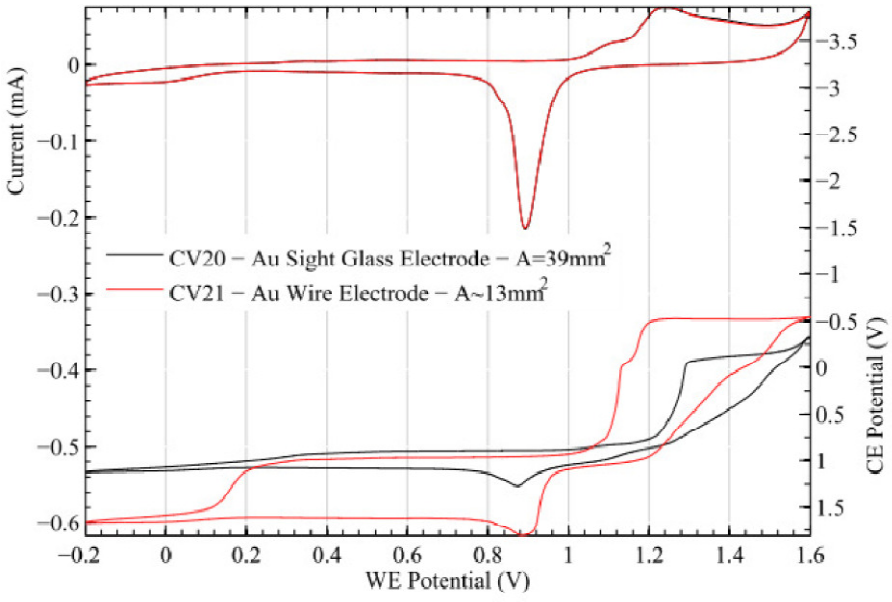

Figure B.5: Comparison of the counter electrode (CE) potential between Au sight glass electrode ($39mm^2$) and Au wire electrode ($13mm^2$) in CV, 0.1M $HClO_4$ as CEs, scan rate: 20mV/s.

Figure B.4 shows a cyclic voltammogram using a 0.1M $HClO_4$ solution (scan rate: 20mV/s) performed in the new electrochemical cell.

Figure B.5 compares the response of two different counter electrodes ($13mm^2$ and $39mm^2$ of contact area). The half process that occurs in the counter electrode should be fast enough to let the process in the working electrode not to be limited. When the area of the counter electrode (CE) is bigger, the potential range on the CE is smaller and the process in the working electrode is less limited.

The main possibilities that this new electrochemical cell allows are: temperature control that can be installed in order to perform dsDNA melting (denaturation) experiments, and, small volume cell in order to reduce the amount of sample required.

Appendix C: Dipoles moment on DNA nucleotides

Another property tightly related with adsorption is the dipole moment of DNA nucleotides. It produces a change in the electrical conditions of the gold-coated cantilever surface shifting the potential of zero charge [17].

It is well-known that the macromolecules have a high dipole moment. In this appendix we discuss the dipole moment present in the thiol functional group, and the dipole moment present in each nucleic-acid. In the case of the entire structure of thiolated DNA (single stranded or double stranded), many factors will determine the value of the total dipole moment: The conformational state, the tilt angle, and the angle of torsion that the strand of DNA has with respect with the thiolated alkane 'connector' surface. All these factors are important to estimate the magnitude and direction of its dipole moment [73].

The normal component of a dipole moment with respect to the gold-coated cantilever surface is the only relevant component that creates a V_{pzc} shift. The normal component induces movement of charges in the surface and the difference in the charge on the surface varies the V_{pzc} [3].

Nucleic-acid	Dipole moment (Debye units)
Adenine	2.49 D
Thymine	3.88 D
Guanine	2.76 D
Cytosine	6.12 D

Table 3.1: Dipole moment of DNA nucleotides. From [79].

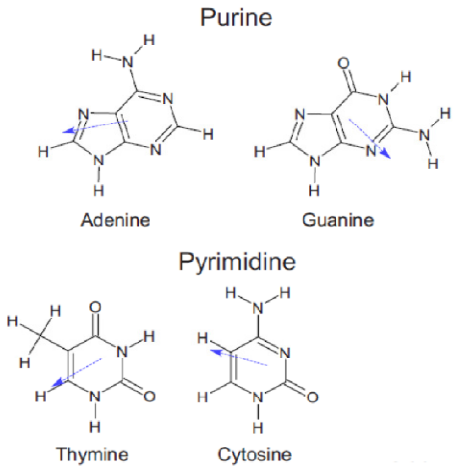

Figure 3.5: Dipole moment orientation of DNA nucleotides. From [72].

Table 3.1 and figure 3.5 show the magnitude and the orientation of the dipole moments of the DNA nucleic-acids (A, T, C, G). The dipole moments present on the ssDNA, dsDNA, and the thiol group changes the electrical conditions of the gold-coated surface of the cantilever. In a similar way, the negatively charged backbone of ssDNA and dsDNA produces changes in the electrical conditions that result in a shift of the potential of zero charge.

The quantitative analysis of the shift of V_{pzc} due to dipole moment of thiolated DNA is not yet performed. Ramirez et al [17] calculated the shift in the potential of zero charge caused by dipole moments present on different thiol monolayers. For the thiol group that we use: heptanethiol, the dipole moment observed is 2.044 Debyes and the new potential of zero charge is -0.45 +/- 0.02 Volts.

The value of the resultant dipole moment varies with the amount of thiolated DNA (ssDNA or dsDNA) on the cantilever surface. As a result, the change in the

adsorption conditions due to a V_{pcz} shift depends strongly on the thiolated DNA surface density of the gold-coated cantilever surface.

References

[1] R. McKendry, J. Zhang, Y. Arntz, T. Strunz, M. Hegner, H. P. Lang, M. K. Baller, U. Certa, E. Meyer, H.-J. Güntherodt and C. Gerber, Proceedings of the National Academy of Sciences of the United States of America **99** (15), 9783-9788 (2002).

[2] M. Nordström, S. Keller, M. Lillemose, A. Johansson, S. Dohn, D. Haefliger, G. Blagoi, M. Havsteen-Jakobsen and A. Boisen, Sensors **8** (3), 1595-1612 (2008).

[3] A. Boisen and et al., Reports on Progress in Physics **74** (3), 036101 (2011).

[4] K. M. Hansen, H.-F. Ji, G. Wu, R. Datar, R. Cote, A. Majumdar and T. Thundat, Analytical Chemistry **73** (7), 1567-1571 (2001).

[5] W. Fritzsche and T. A. Taton, Nanotechnology **14** (12), R63 (2003).

[6] A. K. H. Cheng, D. Sen and H.-Z. Yu, Bioelectrochemistry **77** (1), 1-12 (2009).

[7] J. P. Chambers, B. P. Arulanandam, L. L. Matta, A. Weis and J. J. Valdes, Curr. Issues Mol. Biol. **10**, 1-12 (2008).

[8] A. B. Steel, T. M. Herne and M. J. Tarlov, Analytical Chemistry **70** (22), 4670-4677 (1998).

[9] J. Fritz, M. K. Baller, H. P. Lang, H. Rothuizen, P. Vettiger, E. Meyer, H. -J. Güntherodt, C. Gerber and J. K. Gimzewski, Science **288** (5464), 316-318 (2000).

[10] M. Godin, P. J. Williams, V. Tabard-Cossa, O. Laroche, L. Y. Beaulieu, R. B. Lennox and P. Grütter, Langmuir **20** (17), 7090-7096 (2004).

[11] M. Godin, V. Tabard-Cossa, Y. Miyahara, T. Monga, P. J. Williams, L. Y. Beaulieu, R. B. Lennox and Peter Grutter, Nanotechnology **21** (7), 075501 (2010).

[12] J. C. Stachowiak, M. Yue, K. Castelino, A. Chakraborty and A. Majumdar, Langmuir **22** (1), 263-268 (2005).

[13] M. F. Hagan and A. K. Chakraborty, The Journal of Chemical Physics **120** (10), 4958-4968 (2004).

[14] M. F. Hagan, A. Majumdar and A. K. Chakraborty, The Journal of Physical Chemistry B **106** (39), 10163-10173 (2002).

[15] G. Wu, H. Ji, K. Hansen, T. Thundat, R. Datar, R. Cote, M. F. Hagan, A. K. Chakraborty and A. Majumdar, Proceedings of the National Academy of Sciences **98** (4), 1560-1564 (2001).

[16] G. E. Plum and V. A. Bloomfield, Biopolymers **29** (8-9), 1137-1146 (1990).

[17] P. Ramírez, R. Andreu, Á. Cuesta, C. J. Calzado and J. J. Calvente, Analytical Chemistry **79** (17), 6473-6479 (2007).

[18] U. Rant, K. Arinaga, S. Fujita, N. Yokoyama, G. Abstreiter and M. Tornow, Organic & Biomolecular Chemistry **4** (18), 3448-3455 (2006).

[19] A. Bard and L. Faulkner, *Electrochemical methods: fundamentals and applications*. (Wiley, 2001).

[20] See reference 19, chapter 1 page 12-18, chapter 13.

[21] J. Lipkowski, Z. Shi, A. Chen, B. Pettinger and C. Bilger, Electrochimica Acta **43** (19-20), 2875-2888 (1998).

[22] http://www.argentumsolutions.com/wiki/upload/2008/9/potentiostat-04134516.gif

[23] See reference 19, page 53.

[24] H. Suzuki, H. Shiroishi, S. Sasaki and I. Karube, Analytical Chemistry **71** (22), 5069-5075 (1999).

[25] See reference 19, Page 27 figure 21.23.12.

[26] http://www.spmtips.com/csc/c12/tipless

[27] F. Schreiber, Progress in Surface Science **65** (5-8), 151-257.
[28] http://www.ellsworth.com
[29] V. Tabard-Cossa, *Microcantilever actuation generated by redox-induced surface stress*, in *Department of Physics*. 2006, McGill University: Montreal.
[30] V. Tabard-Cossa, M. Godin, L. Y. Beaulieu and P. Grütter, Sensors and Actuators B: Chemical **107** (1), 233-241 (2005).
[31] M. Ciobanu, J. P. Wilburn, M. L. Krim and D. E. Cliffel, in *Handbook of Electrochemistry*, edited by G. Z. Cynthia (Elsevier, Amsterdam, 2007), pp. 3-29.
[32] http://www.cheng.cam.ac.uk/research/groups/electrochem/JAVA/electrochemistry/ELEC/l4html/cv.html
[33] See reference 19, Page 512-515.
[34] R. S. Nicholson, Analytical Chemistry **37** (11), 1351-1355 (1965).
[35] Y. Golan, L. Margulis and I. Rubinstein, Surface Science **264** (3), 312-326 (1992).
[36] See reference 19, 167-169.
[37] V. S. Bagotsky, *Fundamentals of Electrochemistry*. (Wiley, 2006).
[38] See reference 19, 207-210.
[39] P. Atkins and J. Paula, *Atkins' Physical Chemistry*. (W H Freeman & Co, 2006), 932-936.
[40] See reference 19, 12-14.
[41] See reference 19, 534-580.
[42] See reference 37, 149-150.
[43] J. E. Sader, J. W. M. Chon and P. Mulvaney, Review of Scientific Instruments **70** (10), 3967-3969 (1999).
[44] T. A. Brunt, E. D. Chabala, T. Rayment, S. J. O'Shea and M. E. Welland, Journal of the Chemical Society, Faraday Transactions **92** (20), 3807-3812 (1996).
[45] D. J. Muller and Y. F. Dufrene, Nat Nano **3** (5), 261-269 (2008).
[46] T. Monga, *Surface Stress at the Solid-Liquid Interface: Alkanethiol Monolayers on Gold*, in *Department of Chemistry*. 2006, McGill University: Montreal.
[47] G. G. Stoney, Proceedings of the Royal Society of London. Series A **82** (553), 172-175 (1909).
[48] R. W. Corkery, Langmuir **13** (14), 3591-3594 (1997).
[49] J. C. Love, L. A. Estroff, J. K. Kriebel, R. G. Nuzzo and G. M. Whitesides, Chemical Reviews **105** (4), 1103-1170 (2005).
[50] R. G. Nuzzo, F. A. Fusco and D. L. Allara, Journal of the American Chemical Society **109** (8), 2358-2368 (1987).
[51] T. Aqua, R. Naaman and S. S. Daube, Langmuir **19** (25), 10573-10580 (2003).
[52] R. G. Nuzzo, L. H. Dubois and D. L. Allara, Journal of the American Chemical Society **112** (2), 558-569 (1990).
[53] P. Maksymovych, O. Voznyy, D. B. Dougherty, D. C. Sorescu and J. T. Yates Jr, Progress in Surface Science **85** (5-8), 206-240.
[54] M. Kind and C. Wöll, Progress in Surface Science **84** (7-8), 230-278.
[55] L. Y. S. Lee, T. C. Sutherland, S. Rucareanu and R. B. Lennox, Langmuir **22** (9), 4438-4444 (2006).
[56] C. C. Wildrich CA, Porter MD, (Electroanal Chem, 1991), pp. 310-335.
[57] S. Patai, *The chemistry of the thiol group*. (Wiley, 1974).
[58] J. W. Gibbs, Longmans-Green, Halle, 55 (1906).
[59] H. Ibach, Surface Science Reports **29** (5-6), 195-263 (1997).
[60] H. Ibach, Journal of Vacuum Science & Technology A: Vacuum, Surfaces, and Films **12** (4), 2240-2245 (1994).
[61] A. J. Schell-Sorokin and R. M. Tromp, Surface Science **319** (1-2), 110-118 (1994).

[62] A. M. Moulin, S. J. O'Shea, R. A. Badley, P. Doyle and M. E. Welland, Langmuir **15** (26), 8776-8779 (1999).
[63] A. M. Moulin, S. J. O'Shea and M. E. Welland, Ultramicroscopy **82** (1-4), 23-31 (2000).
[64] W. Haiss, Reports on Progress in Physics **64** (5), 591 (2001).
[65] http://www.operon.com
[66] http://www.gelifesciences.com
[67] F. Silva and A. Martins, Journal of Electroanalytical Chemistry **467** (1-2), 335-341 (1999).
[68] U. Rant, K. Arinaga, S. Fujita, N. Yokoyama, G. Abstreiter and M. Tornow, Nano Letters **4** (12), 2441-2445 (2004).
[69] Y.Nagai, J. Dulanto Carbajal, B. Pietrobon, H. Djamzabian, H. Bourque, J. White, R. Sladek, P. Grutter, and R. B. Lennox (manuscript in progress, 2011).
[70] http://www.invitrogen.com
[71] U. Rant, K. Arinaga, M. Tornow, Y. W. Kim, R. R. Netz, S. Fujita, N. Yokoyama and G. Abstreiter, Biophysical journal **90** (10), 3666-3671 (2006).
[72] M. Zwolak and M. Di Ventra, Reviews of Modern Physics **80** (1), 141 (2008).
[73] K. Sinniah, J. Cheng, S. Terrettaz, J. E. Reutt-Robey and C. J. Miller, The Journal of Physical Chemistry **99** (39), 14500-14505 (1995).
[74] http://www.sigmaaldrich.com
[75] http://www.thermoscientific.com
[76] A. Panjkovich and F. Melo, Bioinformatics **21** (6), 711-722 (2005).
[77] http://www.victrex.com
[78] http://www.ptfeparts.com/teflon.htm
[79] S. Riahi, S. Eynollani, M. R. Ganjali and P. Norouzi, Electrochemical Science **5**, 355-366 (2010).